Article

Cell

# Formation of a Neurosensory Organ by Epithelial Cell Slithering

## Graphical Abstract

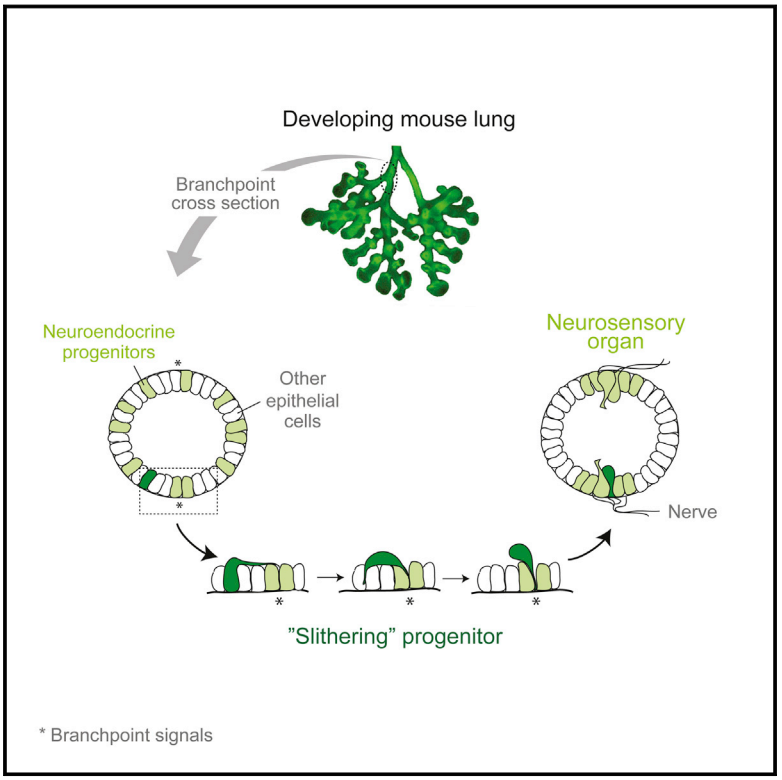


## Authors

Christin S. Kuo, Mark A. Krasnow

## Correspondence

krasnow@stanford.edu

## In Brief

A form of migration named "slithering," where cells undergo transient EMT, allows rapid assembly of pulmonary neurosensory organs and may explain why lung cancers arising from neuroendocrine cells are highly metastatic.

## Highlights

- Neuroendocrine cells form clusters at stereotyped positions at branch junctions
- Progenitors are selected randomly in epithelium but rapidly sort from other cells
- Sorting occurs by directed migration of progenitors to branch junctions
- Migrating cells undergo transient EMT, crawling over neighbor cells to the target

Kuo & Krasnow, 2015, Cell *163*, 394–405
October 8, 2015 
http://dx.doi.org/10.1016/j.cell.2015.09.021

CellPress

Cell

Article

# Formation of a Neurosensory Organ by Epithelial Cell Slithering

Christin S. Kuo[1,2,3] and Mark A. Krasnow[1,3,*]
[1]Department of Biochemistry
[2]Department of Pediatrics
[3]Howard Hughes Medical Institute
Stanford University School of Medicine, Stanford, CA 94305-5307, USA
*Correspondence: krasnow@stanford.edu
http://dx.doi.org/10.1016/j.cell.2015.09.021

## SUMMARY

**Epithelial cells are normally stably anchored, maintaining their relative positions and association with the basement membrane. Developmental rearrangements occur through cell intercalation, and cells can delaminate during epithelial-mesenchymal transitions and metastasis. We mapped the formation of lung neuroepithelial bodies (NEBs), innervated clusters of neuroendocrine/neurosensory cells within the bronchial epithelium, revealing a targeted mode of cell migration that we named "slithering," in which cells transiently lose epithelial character but remain associated with the membrane while traversing neighboring epithelial cells to reach cluster sites. Immunostaining, lineage tracing, clonal analysis, and live imaging showed that NEB progenitors, initially distributed randomly, downregulate adhesion and polarity proteins, crawling over and between neighboring cells to converge at diametrically opposed positions at bronchial branchpoints, where they reestablish epithelial structure and express neuroendocrine genes. There is little accompanying progenitor proliferation or apoptosis. Activation of the slithering program may explain why lung cancers arising from neuroendocrine cells are highly metastatic.**

## INTRODUCTION

Epithelia are sheets of cells that line and protect the body and internal organs, and the polarized cells that comprise them play important roles in absorption, secretion, and sensation. Epithelial cells are normally tightly attached to one another through specialized junctions and adhesion proteins along their lateral surface and anchored to the basement membrane at their basal surface. Although epithelial sheets can grow and change shape, the constituent cells typically maintain their relative positions. When cells in an epithelial monolayer have been found to rearrange, as in *Drosophila* germband elongation (Irvine and Wieschaus, 1994) and wing morphogenesis (Aigouy et al., 2010), they do so conservatively by cell intercalation, in which cells shrink lateral junctions with some neighboring cells while expanding lateral junctions with others, exchanging positions while maintaining their polarized structure and the integrity of the epithelium (Bertet et al., 2004; Blankenship et al., 2006; Guillot and Lecuit, 2013). Here, we describe a very different mode of epithelial cell rearrangement that results in homotypic sorting (Krens and Heisenberg, 2011) of a specialized cell type, discovered in our dissection of pulmonary neuroendocrine (NE) cell development in mice.

Pulmonary NE cells are one of the most interesting but least understood cell types in the lung. They are distributed throughout the bronchial epithelium, interspersed among secretory club (Clara) cells and ciliated cells, the two major airway epithelial cell types (Rock and Hogan, 2011). Like other neuroendocrine cells in the body, they were originally identified by their secretory dense-core vesicles (Feyrter, 1954) that contain signaling molecules and bioactive peptides, including serotonin and calcitonin gene-related peptide (CGRP). Although some pulmonary NE cells are distributed randomly in the airway epithelium, others are organized into clusters called neuroendocrine or neuroepithelial bodies (NEBs) that are highly innervated (Brouns et al., 2009; Lauweryns and Peuskens, 1972), forming synaptic contacts with afferent and efferent nerve fibers (Lauweryns and Van Lommel, 1987). NE cells can be activated by a variety of stimuli and are thought to monitor diverse aspects of lung physiology including oxygen, chemical, and mechanical changes (Cutz et al., 2013). In addition to these sensory and neurosecretory functions, NE cells have a stem cell function that helps replenish the bronchial epithelium following severe injury (Guha et al., 2012; Reynolds et al., 2000; Song et al., 2012). They are also the initiating cells of small cell lung cancer (Park et al., 2011; Song et al., 2012; Sutherland et al., 2011), a highly metastatic and the most deadly form of lung cancer (van Meerbeeck et al., 2011). Excess or altered distribution of NE cells are also found in a variety of serious, but poorly understood, lung diseases including sudden infant death syndrome (SIDS) (Cutz et al., 2007), bronchopulmonary dysplasia (BPD) (Gillan and Cutz, 1993), and neuroendocrine hyperplasia (Aguayo et al., 1992; Deterding et al., 2005).

To provide a foundation for a genetic dissection of the development, function, and diseases of pulmonary NE cells, we first mapped their locations in mice and found that NEBs are located at stereotyped positions. We then probed NEB development by

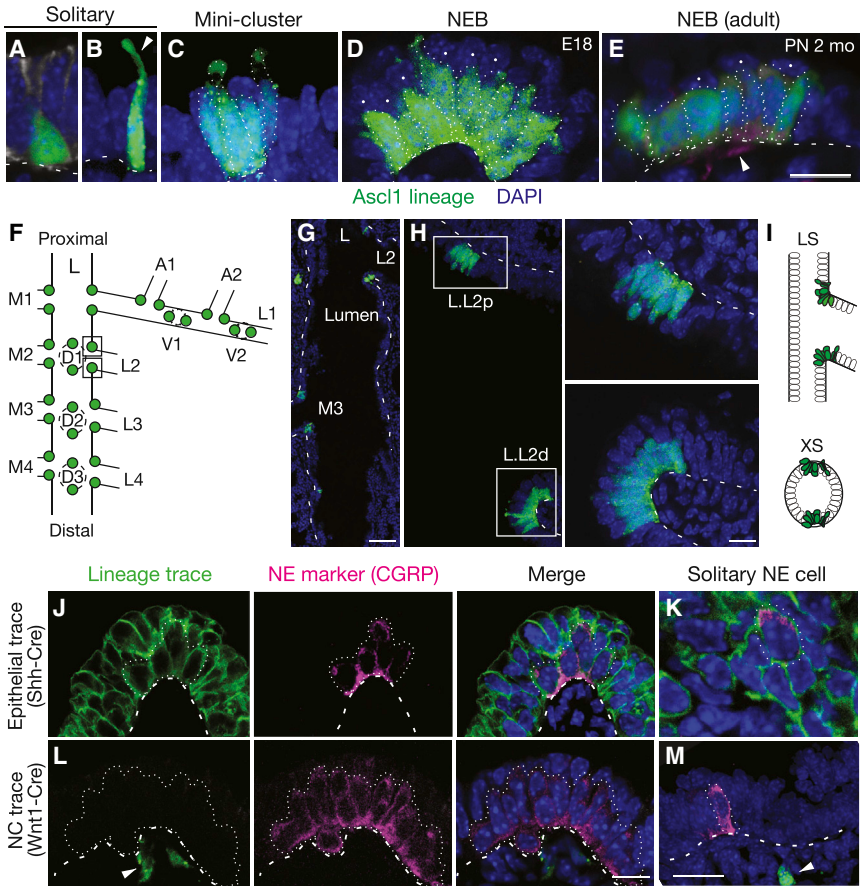


**Figure 1. Mapping and Lineage Tracing of Pulmonary Neuroendocrine Cells**

(A–E) Confocal images of NE cells in bronchial epithelium of embryonic day (E) 18 (A–D) or adult (postnatal 2 month; E) *Ascl1*$^{CreER/+}$; *Rosa26*$^{ZsGreen/+}$mouse induced with tamoxifen at E14 to label NE cells with ZsGreen (green). See also Figure S1. (A and B) Solitary NE cells with pyramidal (A) and slender (B) morphologies. Arrowhead, thin projection to lumen. (C) Mini-cluster of four NE cells. (D) Neuroepithelial body (NEB), a large cluster of ~25 NE cells (12 visible in optical plane). (E) Adult NEB. Cells are more uniformly columnar. Note non-NE cells (nuclei marked by dots) superficial to NE cells in NEBs (D and E). Sample was also stained with PGP9.5 (red) to confirm NE identity and show innervating fibers (arrowhead). Dotted lines, individual NE cells in clusters; dashed lines, basement membrane location determined by co-staining with E-cadherin or laminin γ1. Scale bar, 10 μm.

(F–I) Stereotyped locations of NEBs at airway branchpoints. (F) Left primary bronchus (L) and some daughter (L.L1, L.L2, …) and granddaughter (L.L1.A1, L.L1.A2,…) branches showing positions of NEBs at E18. (G) Low magnification confocal image of left primary bronchus of E18 *Ascl1*$^{CreER/+}$; *Rosa26*$^{ZsGreen/+}$ mouse. Note pairs of NEBs (green) at indicated branch points (L.L2, L.M3), with one NEB located proximal (p) and the other distal (d) along bronchial tree. Scale bar, 100 μm. (H) Longitudinal optical section through base of L.L2 showing L.L2p and L.L2d NEBs. Close-ups of NEBs (boxed) are shown at right. Scale bar, 5 μm. (I) Schematic longitudinal section (LS) and cross section (XS) showing diametrically opposite positions of L.L2 NEBs at branch base. See also Figure S2.

(J–M) Lineage tracing of NE cell origins. Confocal images of NEBs (J and L) and solitary NE cells (K and M) at E18 from *Shh*$^{Cre/+}$;*Rosa26*$^{mTmG/+}$ mouse to label bronchial epithelial lineage (J and K) or from *Wnt1-Cre;Rosa26*$^{ZsGreen/+}$ mouse to label neural crest lineage (L and M). Lungs were co-stained for lineage tag (green) and NE marker CGRP (magenta). All NEB and solitary NE cells express bronchial trace and none express neural crest trace. Other epithelial cells also express bronchial trace, and sub-epithelial neurons (arrowheads) express Wnt1 trace. Dots, outline of NEBs or individual NE cells; dashes, basement membrane. Scale bar, 10 μm.

immunostaining, lineage tracing, and imaging of developmental intermediates and found that although progenitors are initially distributed randomly throughout the epithelium, they rapidly resolve into clusters. We show that clusters do not form by progenitor proliferation, but by a targeted mechanism of epithelial cell rearrangement in which progenitors transiently lose epithelial character as they "slither" over and around neighboring cells and converge at cluster sites.

## RESULTS

### Mapping the Origin and Distribution of NEBs

Pulmonary NE cells are distributed sparsely throughout the bronchial epithelium both as solitary cells and clusters. Most mature NE cells are typical columnar epithelial cells, however, some have distinct morphologies such as short "pyramidal" cells that do not reach the surface or slender cells with a thin luminal projection (Figures 1A and 1B). Clusters are either small, typically with two to five NE cells, which we call "mini-clusters" (Figure 1C), or are larger clusters typically containing 20–30 NE cells (Figures 1D and 1E). The terms "neuroepithelial body" (NEB) and "neuroendocrine body" often refer to all NE cell clusters, but here, we reserve the term NEB for large clusters. NE clusters in other species are innervated (Lauweryns and Peuskens, 1972; Scheuermann, 1987), and we found by immunostaining for neurites with PGP9.5 (Uchl1) that mouse NEBs are extensively innervated and mini-clusters show some innervation, whereas solitary NE cells do not appear to be innervated.

We mapped the locations of NE cells in the mouse bronchial tree in late stage embryonic lungs (embryonic days E16–E18) using the airway branch lineage (Metzger et al., 2008). NE cells were detected by immunostaining for the proneural bHLH transcription factor Ascl1 (Mash1) or cytoplasmic NE marker PGP9.5, or using an *Ascl1*$^{CreER}$ lineage trace, which within the bronchial epithelium labels exclusively the NE lineage (Figure S1). We analyzed serial sections of left lung lobes co-stained for E-cadherin to visualize airway epithelium. Solitary NE cells and mini-clusters were scattered throughout the bronchial epithelium in no obvious pattern. The pattern of NEBs, however, was highly stereotyped. NEBs localized exclusively to airway branchpoints

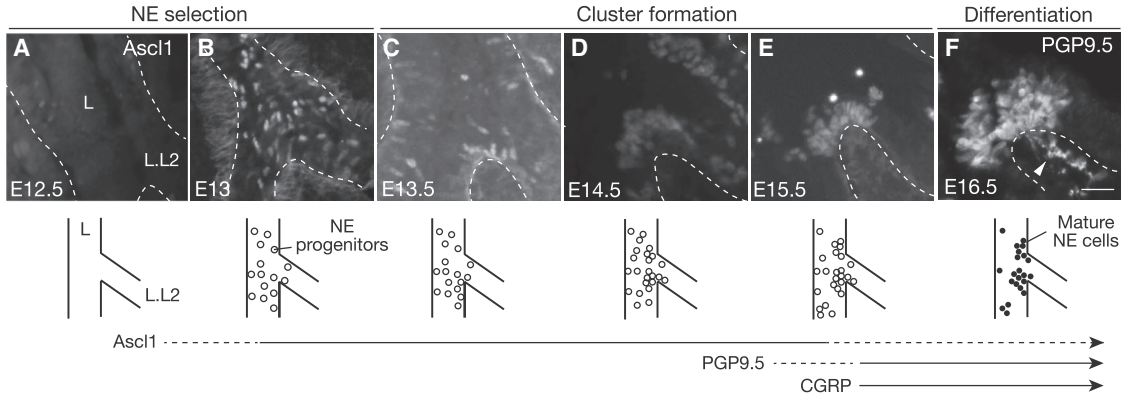


**Figure 2. Cellular Events in NEB Formation**

Longitudinal optical sections and schematics of base of L.L2 bronchus at stages indicated in wild-type lungs stained for NE progenitor marker Ascl1 (A–E) or mature marker PGP9.5 (F). Dashed lines, basement membrane. Three phases of NEB development are indicated: NE cell selection in bronchial epithelium, as indicated by expression of Ascl1 (open circles); NE cell cluster formation at NEB sites; and differentiation marked by expression of PGP9.5 (filled circles) and CGRP (see Figure S3F). Timing of Ascl1, PGP9.5, and CGRP expression is indicated below. PGP9.5-positive nerve fibers (arrowhead, F) extend toward and begin to ramify on L.L2 NEB at E16.5. Scale bar, 25 μm. See also Figure S3.

(Figures 1F and 1G). Although none were found at the origin of the trachea or right and left primary bronchi, at every branchpoint examined beyond this a pair of NEBs was present (Figures 1F, 1G, and S2). NEBs were located at diametrically opposite positions at branch junctions, with one at the most proximal position and the other the most distal (Figures 1H and 1I). Hence, we designate each NEB by the name of the branch it originates, plus "p" or "d" to distinguish proximal and distal partners. The proximal NEB marks the most obtuse angle of the branch junction, whereas the distal NEB lies at the most acute angle. The same pattern was observed at every branchpoint examined in other lobes (Figure S2) (n = 5 lungs, 70 branchpoints). Thus, NEBs form at stereotyped, diametrically opposite positions at secondary airway branchpoints and beyond, implying there is a localized signal directing NEB formation at each of these sites.

NE cells in other organs arise either from invading neural crest cells that colonize the organ or by differentiation of resident epithelial cells (Anderson and Axel, 1986; Gu et al., 2002). Initial lineage trace studies indicated that at least some pulmonary NE cells arise from the epithelium (Song et al., 2012). To determine if NEBs arise from the epithelium, we used a *Sonic hedgehog*$^{Cre}$ (*Shh*$^{Cre}$) knock-in allele (Harris et al., 2006) and a Cre recombinase reporter to label and lineage trace developing airway epithelial progenitors several days before NE progenitors are detected. At E18.5, all NEBs as well as mini-clusters and solitary pulmonary NE cells expressed the *Shh*$^{Cre}$ lineage trace (n = 500 NE cells scored) (Figures 1J and 1K). In a similar experiment using a *Wnt1-Cre* transgene to lineage trace developing neural crest cells, no NE cells at E18.5 expressed the lineage trace (n = 500) (Figure 1L). We conclude that all pulmonary NE cells, including NEBs, arise from the *Shh* epithelial lineage, not from neural crest. Thus, both solitary and clustered pulmonary NE cells share the same origin as other airway epithelial cells.

## Three Phases of NEB Development

To elucidate the cellular events and timing of NEB formation, we mapped the development of specific NEBs beginning at E12, before NE progenitors are detected, through E16 when NEBs achieve their characteristic structure. We used Ascl1, the earliest known marker of NE cells (Ito et al., 2000), to visualize progenitors and early events and PGP9.5 and CGRP, canonical markers of mature NE cells (Polak et al., 1993), to visualize later steps. We analyzed five serially sectioned wild-type CD-1 lungs at each of six stages between E12–E16, initially focusing on the base of branch L.L2 where NEBs L.L2p and L.L2d form (Figure 2). The earliest NE progenitors at these sites were detected at late E12.5–E13, when a few scattered cells in the epithelium began to express Ascl1 (Figure 2A). At E13, more densely distributed but still solitary NE progenitors were present in a "salt and pepper" pattern (Figure 2B). By late E13.5–E14, small groups of NE progenitors were detected at L.L2p and L.L2d and also scattered around the region (Figure 2C). By E14.5, within 24–48 hr of detection of the first NE progenitors, numerous small clusters of NE cells began to appear throughout the region, interspersed with solitary cells (Figures 2D and S3B). At E15.5, large clusters of NE cells were detected, but exclusively at the positions of NEBs L.L2p and L.L2d (Figure 2E). By E15.5–E16, NE cells in NEBs L.L2p and L.L2d expressed PGP9.5 and CGRP, as did solitary NE cells and mini-clusters in the region (Figures 2F, S3E, and S3F). This analysis subdivided NEB formation into three developmental phases: NE cell selection (E12.5–E13.5), cluster formation (E13.5–E15.5), and differentiation (E15.5 onward). During differentiation, PGP9.5-positive nerve fibers extend toward and begin to ramify on the NEB (Figures 2F and S3G–S3I).

The same series of cellular events and developmental phases was observed at other positions where NEB formation was mapped, including L.L3p/L.L3d, L.L4p/L.L4d, and L.L5p/L.L5d, all located at the base of secondary branches along the left primary bronchus. However, the process initiates slightly later at the more distal positions, delayed by ~0.5 day for L.L3, 1 day for L.L4, and 1.5 days for L.L5 NEBs. This is best appreciated in images capturing all four positions in the same lung, when the most distal branch (L.L5) has not yet initiated NE development, L.L4 is

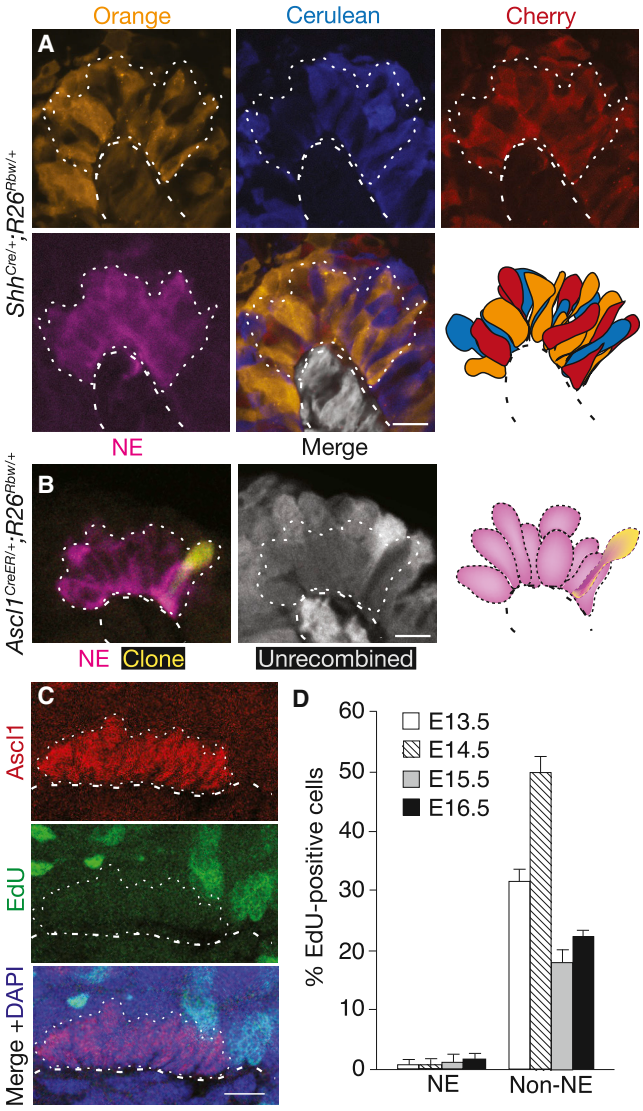


**Figure 3. Analysis of Proliferation during NEB Formation**

(A) Close-up of NEB in *Shh*$^{Cre/+}$;*Rosa26*$^{Rbw/+}$ mouse lung in which entire bronchial epithelium was permanently labeled with one of the Rainbow reporters (Orange, Cerulean, or Cherry) before NE selection then co-stained for CGRP (magenta) at E18 following NEB formation. NEB (dotted outline) is composed of cells labeled with each of the reporters, thus it did not arise by proliferation of a single progenitor. Epithelial cells neighboring the NEB are not shown in schematic; cells below basement membrane (dashed line) express the constitutive (expressed in absence of Cre) GFP reporter (pseudo-colored gray). Scale bar, 10 μm. See also Table S1.

(B) Close-up of a NEB in E18 *Ascl1*$^{CreER/+}$;*Rosa26*$^{Rbw/+}$ mouse lung in which NE progenitors were sparsely labeled by injection of tamoxifen (4 mg) early in NE development (E11.5) then immunostained for CGRP (magenta) 6 days later following NEB formation. Note one labeled cell (pseudocolored yellow) in NEB, indicating that labeled progenitor did not proliferate. Cells without Cre activity ("Unrecombined") express the GFP reporter (pseudo-colored gray in middle panel); note absence of GFP in clone (yellow cell). Only cells in NEB (dotted lines) are shown in schematic. Scale bar, 10 μm. See also Tables S2A–S2C.

(C) Confocal sagittal section through cluster of NE cells during NEB formation in E14 wild-type embryo in which EdU was injected 2 hr before harvesting to label dividing cells, then analyzed after co-staining for EdU (green) and Ascl1 (red). No NE cells, but many surrounding epithelial cells, are labeled with EdU.

(D) Quantification of EdU-positive NE and non-NE airway epithelial cells at indicated ages. Values shown are percent ± SE for proportions (n = 134, 119, 78, 130 [NE cells], n = 520, 322, 326, 930 [non-NE cells] at E13.5, 14.5, 15.5, 16.5, respectively) scored in two embryos for each cell type scored at each age. Note few EdU-positive NE cells, indicating progenitors exit cell cycle at or just after selection. Similar results were obtained for phospho-histone H3 analysis. Scale bar, 10 μm.

undergoing NE cell selection, L.L3 has begun NE clustering, and L.L2 is in the NE differentiation phase (Figures S3A and S3B). Thus, NEBs form in three phases—NE selection, cluster formation, and differentiation—that initiate in a proximal-to-distal sequence separated by approximately a half day between branches along the left primary bronchus. Despite differences in the timing of NEB program initiation along the proximal-distal axis, the differentiation phase begins in near synchrony for all NEBs and other NE cells (Figures S3G–S3I), suggesting that this final phase is triggered by a more global signal independent of earlier steps in the program.

## Cluster Formation Does Not Occur by Proliferation of NE Precursors

NE and neurosensory cells in many tissues are arranged in clusters, but how clusters form is only understood for *Drosophila* and other insect sensory bristles. Each *Drosophila* bristle arises by proliferation of a single progenitor expressing Achaete-Scute proteins (founders of the *Ascl1* gene family), and the clonal cell cluster differentiates into bristle sensory and support cells (Cubas et al., 1991; Lawrence, 1966). To determine if NEBs form by clonal proliferation of an epithelial progenitor, we labeled all airway epithelial progenitors prior to NEB formation using *Shh*$^{Cre}$ and the "Rainbow" (*Rosa26*$^{Rbw}$) Cre-reporter (Rinkevich et al., 2011), which stochastically and permanently labels each progenitor and any of its daughter cells with one of three different fluorescent proteins. If NEBs form like *Drosophila* sensory bristles, each mature NEB should be monoclonal and hence composed of cells of a single Rainbow color. We found instead that all NEBs examined at E17.5–E18 (n > 100), including those examined closely by confocal microscopy to distinguish individual NE cells, were multi-colored (Figure 3A; Table S1). A similar result obtained for NE miniclusters. Thus, NEBs and miniclusters arise from multiple founder cells, not clonal proliferation of a single NE progenitor.

Although the above results rule out NEB formation by proliferation of a single progenitor, they do not exclude the possibility that NEBs are polyclonal, arising by proliferation of multiple NE progenitors. We therefore carried out two types of experiments to investigate the role of progenitor proliferation in NEB formation. We first used an inducible Cre recombinase (Cre-ER) expressed from the endogenous *Ascl1* promoter (*Ascl1*$^{CreER}$) (Kim et al., 2011), and an early (~E11.5–E12) dose of the inducer tamoxifen, to sparsely label individual NE progenitors with one of the Rainbow colors. When mature NEBs and miniclusters were examined 6 days later, few clusters were labeled, and of those that were, most contained just a single labeled cell (30 of 39 labeled clusters) (Figure 3B). In those with more than one labeled

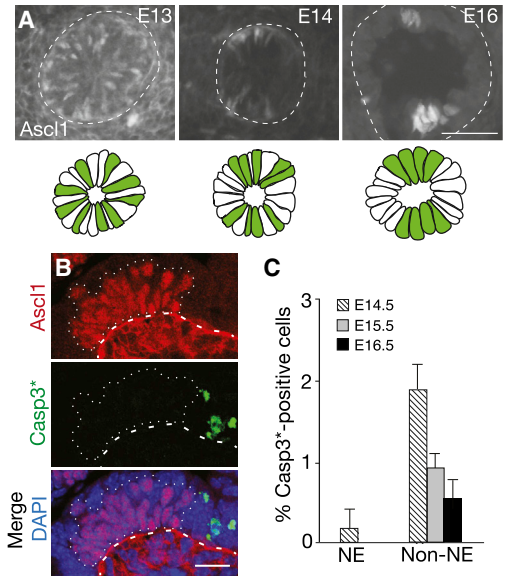


**Figure 4. Local Clearing of NE Cell Precursors during Cluster Formation**

(A) Cross-sections through base of bronchial branch L.V2 at indicated ages of wild-type embryos immunostained for Ascl1 (white; green in schematics below) to show NE progenitors forming NEBs L.V2p and L.V2d. Progenitors are initially scattered in "salt and pepper" pattern but, as NEBs form, surrounding regions clear of NE cells. Scale bar, 10 μm.

(B) Sagittal section through developing NEB (dotted outline) in E14 lung co-stained for Ascl1 (red) and activated (cleaved) Caspase 3 (Casp3*, green) to detect apoptotic cells. Note Casp3*-positive cells near, but not within, NEB (dotted outline). Ascl1 signal below basement membrane (dashed line) at E13 and E14 is non-specific background. Scale bar, 10 μm.

(C) Quantification of Casp3*-positive NE and non-NE cells in bronchial epithelium at indicated stages. Data shown are percent ± SE for proportions; n = 589, 406, 322 (NE cells), 1,437, 1,534, 1,122 (non-NE cells) scored at E14.5, 15.5, 16.5, respectively, from two embryos at each stage.

cell, the cells were usually different colors, in the ratio expected for independent labeling events (Table S2). These clonal labeling results imply that there is little or no proliferation of NE progenitors once they express the progenitor marker Ascl1. A similar conclusion obtained by pulse-labeling with deoxyribonucleotide analog EdU from E12–E15 to detect dividing NE cells. Although EdU-labeled cells were readily detected in surrounding (non-neuroendocrine) epithelial cells and mesenchyme, few labeled NE cells were detected (Figures 3C and 3D). The only labeled NE cells (<1% of NE cells) were solitary NE progenitors in the most distal regions of the bronchial tree just initiating *Ascl1* expression. We conclude that NE progenitors cease dividing at or shortly after initiation of *Ascl1* expression, and proliferation of progenitors does not contribute significantly to cluster formation.

## Local Clearing of NE Cell Precursors without Apoptosis

Inspection of the airway epithelium immediately surrounding positions where NEBs form showed local "clearing" of NE progenitors: progenitors were initially evenly distributed in a salt and pepper pattern like other regions, but labeled cells were lost as NEBs formed nearby (Figure 4A). To determine if clearing was due to programmed cell death, we examined the regions for expression of the apoptosis marker, activated Caspase-3. Although activated Caspase-3 was detected in other developing cell types, little or none was detected in Ascl1-expressing NE progenitors (Figures 4B and 4C). Cell counts also showed no decline in NE progenitors during cluster formation (Figures S3C and S3D). Thus, apoptosis does not contribute to clearing of NE progenitors from regions surrounding NEB formation.

## Sparse Labeling Reveals a Series of Migratory NE Intermediates

Local clearing of progenitors and declining number of solitary NE cells as the number of clustered cells and size of the clusters increased (Figures S3C and S3D) suggested that NEB formation might occur by local sorting of NE progenitors. To identify and visualize developmental intermediates, we sparsely labeled NE progenitors at E11.5 or E12.5 using *Ascl1*$^{CreER}$ and limiting tamoxifen in conjunction with the *Rosa26*$^{ZsGreen}$ reporter that robustly labels NE progenitors, allowing visualization of the full structure of individual intermediates (Figures S4 and S5). Examination of labeled progenitors 2–4 days later (Figure 5A) revealed a collection of developmental intermediates with striking migratory morphologies, including long cytoplasmic extensions, fibroblast-like shapes oriented orthogonal to neighboring epithelial cells—some fully detached from the basement membrane—and cells spiraling around each other and converging at the basement membrane (Figures 5B–5F). NE cells with migratory structures were abundant in regions surrounding sites of NEB formation, and they were transient intermediates detected only during NEB formation (labeling between E12 and E13 but not at E14 or later) that "chased" into mature NEBs in the 36 hr after labeling. The migratory morphologies were specific to the NE lineage as other epithelial cells labeled during this period using *FoxA2*$^{CreER}$ showed the typical structure of monolayer or pseudostratified epithelial cells (Figure S6).

Analysis of over 180 labeled NE intermediates (Table S3) by confocal microscopy distinguished five morphologic classes. Class 1 cells were the earliest and simplest intermediates: solitary NE cell progenitors lacking extensions or unusual morphologic features (Figure 5B). They are early progenitors, presumably before migration has occurred, as they were the only labeled cells detected during the earliest pulse-chase interval (E11.5–E13.5). Class 5 intermediates were similar in structure to Class 1 cells, each showing normal epithelial structure and orientation, except class 5 cells were found in clusters (Figure 5F). Class 5 cells are the most advanced intermediates because they were the only type detected at E16.5 and later (Figure 5G). The other three classes had migratory morphologies and were the most striking and unusual structures. Class 2 intermediates are solitary and resemble class 1 intermediates with a largely normal epithelial morphology, except they have a long (up to 30 μm) cellular extension that reaches over or around neighboring epithelial cells, typically contacting another NE cell several cell diameters away (Figure 5C; Table S3). Class 3 intermediates have the most surprising structure, betraying their epithelial origin. They resembled fibroblasts and had protrusions and often twisted morphologies that curved over or around, and occasionally under, neighboring epithelial cells. Some had no

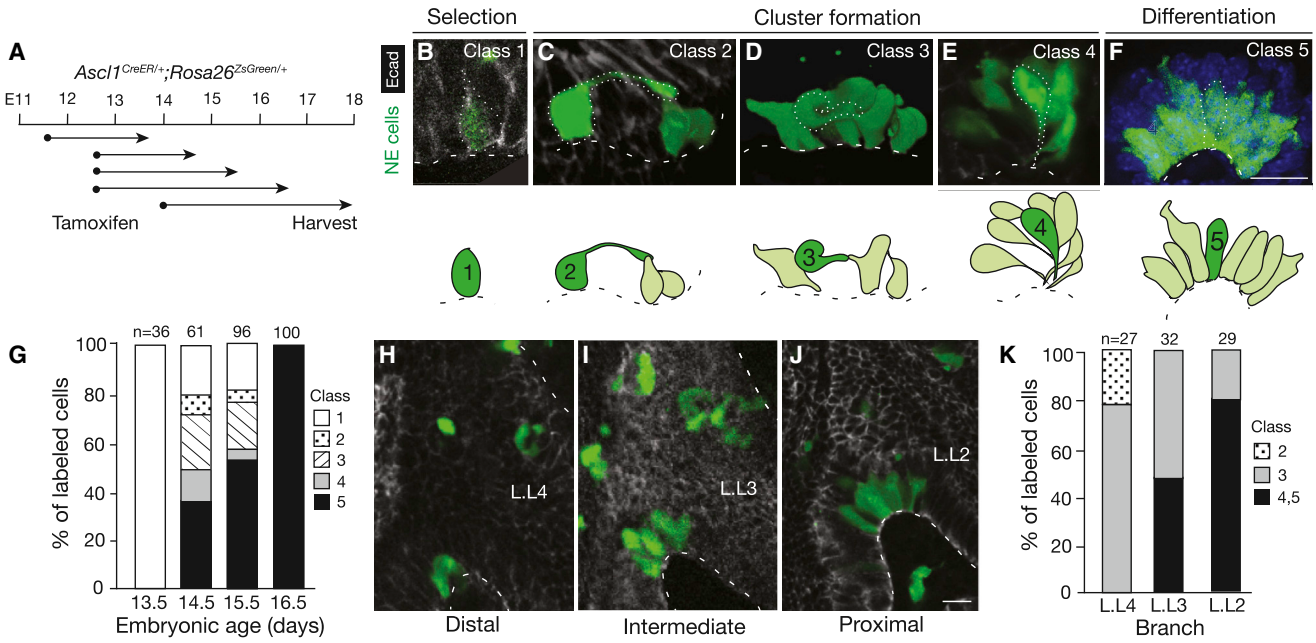


**Figure 5. Sparse Labeling of Progenitors Reveals a Series of NEB Intermediates**

(A) Labeling scheme. NE progenitors were permanently labeled with ZsGreen by tamoxifen injection of *Ascl1*$^{CreER/+}$;*Rosa26*$^{ZsGreen/+}$ mice at indicated ages (dots), then allowed to develop for times indicated (arrows).

(B–F) Micrographs and schematics of five classes of NE intermediates (green) labeled as above and co-stained for E-cadherin to outline epithelial cells. A representative cell of each class is outlined (dots) in micrograph and highlighted in dark green in schematic; other labeled NE cells are shown in light green in schematic. Note long (>10 μm) apical cell extension (class 2), fibroblast-like morphology and no basement membrane contact (class 3), and thin cellular extensions that converge at basement membrane (class 4). In late embryo (~E17) through adult, all NE cells contact basement membrane (class 5). Scale bar, 10 μm. See also Figures S4, S5, and Table S3.

(G) Quantification of different classes of NEB intermediates labeled as above and harvested 48 hr after tamoxifen injection at ages indicated. The changing abundance of intermediates supports their ordering in a developmental series. n, number of intermediates scored in two lungs at each stage.

(H–K) Confocal images (sagittal sections; H–J) and quantification (K) of NEB intermediates labeled as above at base of bronchi L.L4, L.L3, and L.L2 in same lung. L.L4 is most distal (immature) and L.L2 is most proximal (mature) position. The different abundance of intermediates along proximal-distal axis supports their ordering in a developmental series. n, number of intermediates scored in two embryos. Scale bar, 10 μm.

See also Figure S6.

detectable contact with the basement membrane, or contacted it only via a thin cellular extension (Figure 5D). Class 4 intermediates were associated with other NE cells, organized into nascent clusters with cell bodies localized apically and thin extensions swirling as they converged at a site on the basement membrane (Figure 5E).

We inferred from the structures of the intermediates that they comprise a developmental series, beginning with class 1 and proceeding sequentially to class 5 (Figure 7A): NE progenitors first extend long processes and move toward their target at a branch junction, losing their epithelial structure and adopting a mesenchymal morphology as they leave their birth site. They then migrate to the target, converging there with other progenitors and re-establishing their epithelial structure and organizing into clusters. Similar intermediates were observed at sites of mini-cluster formation (Table S3), suggesting that miniclusters form by a related sorting process.

The timing and location of intermediates at sites of NEB formation support the proposed sequence. Quantification of the abundance of each type of intermediate at the same site (along the primary left lobe bronchus) but different times in NEB development (E13.5–E16.5; Figure 5G), or at different stages in the developmental process (represented by different positions along the proximal-distal axis (L.L4, L.L3, L.L2) at the same time in development (E14) (Figures 5H–5K), supported the proposed order. Class 5 intermediates were also the only ones innervated, confirming they are the most mature. Marker expression patterns provide further support for the proposed sequence, with expression of progenitor marker Ascl1 present in class 1 and 2 but progressively declining in class 3, 4, and 5 cells, and expression of late NE markers initiating in class 4 (PGP9.5) and 5 (CGRP) cells (Figures 2, 7A, and 7B).

## Live Imaging of NE Migration during Cluster Formation

To investigate dynamics of progenitor migration and sorting, we developed a slice culture preparation from transgenic *Ascl1*$^{CreER/+}$;*Rosa26*$^{ZsGreen/mTmG}$ embryonic mouse lungs with NE progenitors labeled with ZsGreen and membrane GFP (mGFP) and other cells labeled with mTomato. This allowed tracking by time-lapse confocal microscopy of individual NE progenitors for 2–3 days in the 175-μm thick lung slices as they moved toward and integrated into target sites. This showed

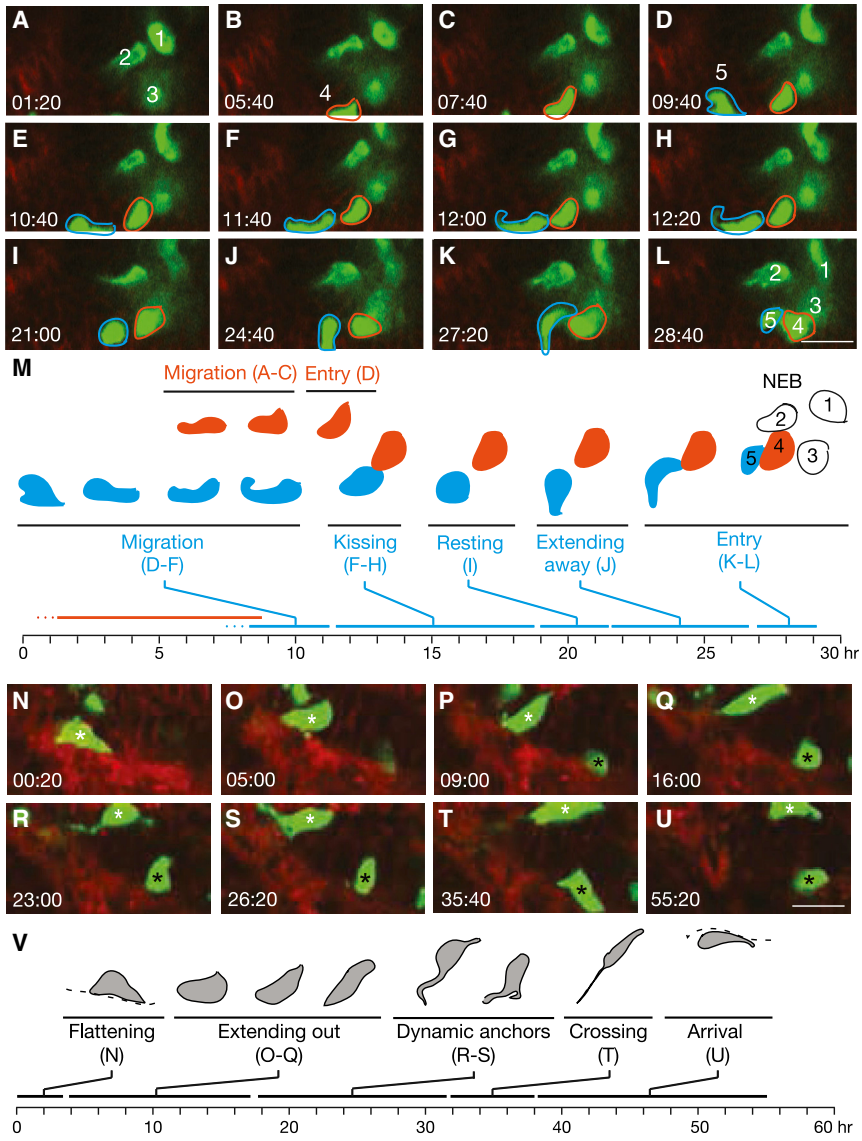


**Figure 6. Live Imaging of Migrating NE Progenitors in Lung Slice Culture**

(A–L) NE cell migration and entry into NEB. Selected frames from 26 hr time-lapse confocal microscopy (Movie S1) of migrating NE cells in E15 mouse lung slice culture from *Asc1*$^{CreER/+}$; *Rosa26*$^{ZsGreen/mTmG}$ mouse induced with tamoxifen at E13 to label NE cells with ZsGreen and mGFP (green) and other cells with mTomato (red). NE cells 1–3 at developing NEB site are joined by cell 4 (red outline), which migrates into region (B and C; at ~1.6 μm/hr) and directly enters cluster (D). Cell 5 (blue outline) migrates into same region (D; ~1.6 μm/hr) but soon changes direction and extends toward cell 4 (E). Cell 4 reciprocates (F) and the cells contact briefly (G, "kissing") and retract (H), repeating kissing sequence four times in ~5 hr. Over the next 5 hr, cell 5 remains stationary (I, "resting") before extending backward (J, "extending away") and then diving forward (K, "entry") to join NEB cluster (L).

(M) Timeline of above changes in cell 4 (red) and 5 (blue).

(N–U) NE cell crossing bronchial tube. Selected frames from another region of same culture. Initially, NE cell (marked with white asterisk) flattens along basement membrane (N, "flattening") then re-orients toward lumen (O-Q, "extending out"). Over next ~14 hr, its contact with basement changes dynamically (R and S, "dynamic anchors"), including formation of a second extension that contacts basement membrane >10 μm away (S). Just before crossing, anchor is a very fine projection with "beaded" appearance (T) that fragments as cell finally crosses (~2.5 μm/hr) into epithelium of opposing side of tube (crossing, T) to reach destination (U, arrival). Frame U was selected from a z plane 8 μm deeper than (N)–(T) to more clearly visualize cell after arrival. Dashed line, basement membrane. Black asterisk, stationary NE cell. Scale bars, 10 μm. See also Movies S1 and S2.

(V) Timeline of above changes in NE cell marked with white asterisk.

progenitors migrating toward targets at 1–3 μm/hr, dynamically extending processes and changing shape as they crawled over and around neighboring epithelial cells (Figures 6A–6M; Movie S1). Progenitors migrated tens of microns or more, traversing many neighboring epithelial cells or even crossing from one side of a developing bronchial tube to the other when the sides were apposed (Figures 6N–6V; Movie S2). Periodically, the migrating cells paused ("resting," Figures 6I and 6M; Movie S1) or changed direction (Figure 6J, "extending away"; Movie S1), or displayed dynamic interactions with other NE cells ("kissing," Figures 6F–6H; Movie S1) or the basement membrane ("dynamic anchors," Figures 6R and 6S; Movie S2). After the progenitor approached the target, this slow and halting migration phase was followed by direct and rapid (~5 μm/hr for 2 hr) entry into the developing cluster. Live imaging confirmed this mode of NE cell migration predicted by the in vivo intermediates, and it revealed dynamic "exploratory" behaviors and interactions with other NE cells and the basement membrane as migrating cells seek and ultimately converge at the target.

## Transient Downregulation of Epithelial Adhesion and Polarity in Migrating Progenitors

The intermediates and movements imply that NE progenitors undergo changes in adhesion and polarity as they migrate and form a NEB. To begin to elucidate the underlying molecular events, we immunostained intermediates for adhesion and polarity markers (Figures 7A and 7C–7E). E-cadherin showed dynamic changes in expression during cluster formation (Figures 7A and 7C). The adhesion protein was expressed at normal levels in early progenitors but dramatically downregulated in migrating class 3 intermediates. Downregulation was transient because E-cadherin was again detected in class 5 intermediates that reached their target and re-established full contact with the basal lamina, although even then E-cadherin levels remained below that of

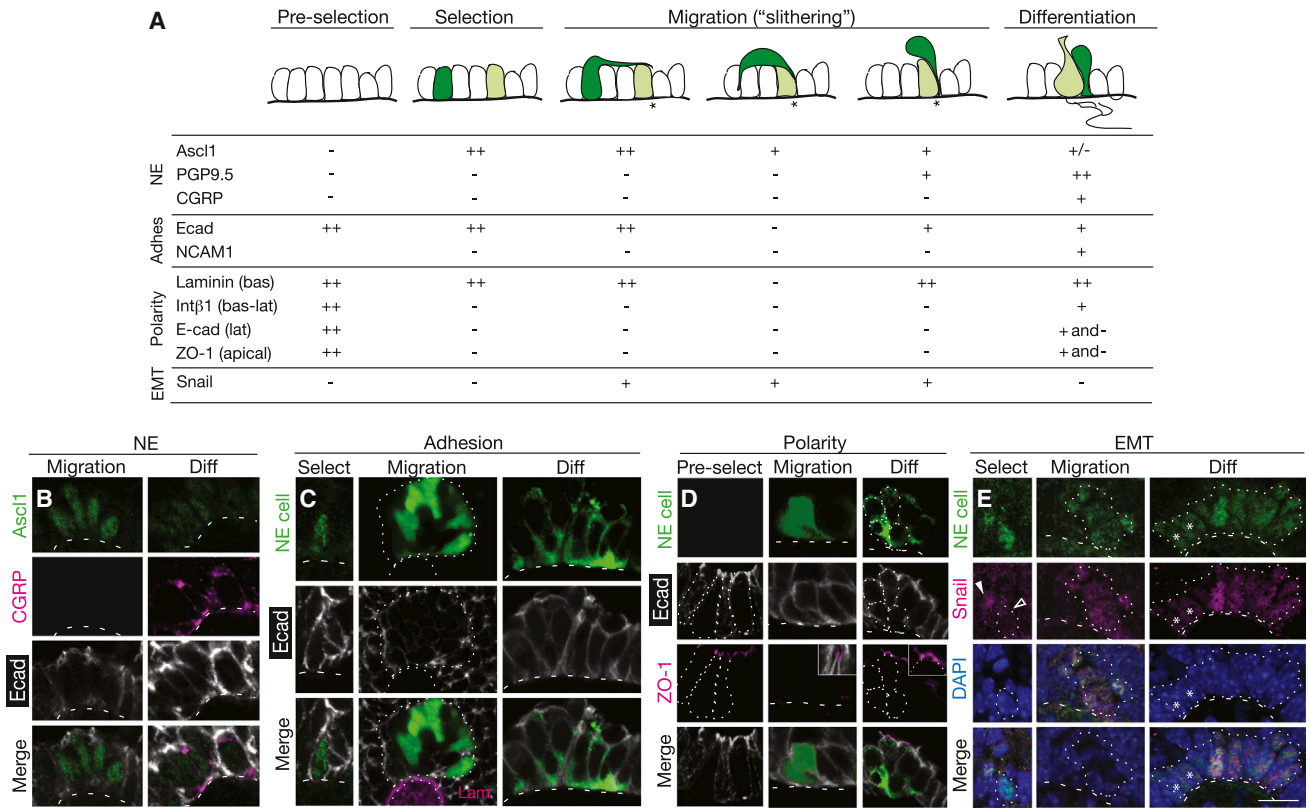


**Figure 7. NE Progenitors Transiently Express EMT Regulator Snail and Downregulate Adhesion and Polarity Markers**

(A) Expression of NE, adhesion (adhes), polarity, and EMT markers in NEB progenitors and intermediates (dark green) at steps indicated: before NE selection (pre-selection) and during NE selection (class 1), migration to form clusters (classes 2–4), and differentiation (class 5). Light green cells, maturing NE cell already at target (asterisk); white cells, NE cells before selection and other non-NE epithelial cells. Symbols show high (++), intermediate (+), low (+/−), no (−), or mixed (+ and −) expression. For polarity markers, expression refers to expression restricted to basal (bas), basolateral (bas-lat), or apical domains. See also Figure S7.

(B–E) Confocal micrographs showing dynamic patterns of indicated NE (B), adhesion (C), polarity (D), and EMT (E) markers at indicated steps of NEB formation. Dots, outline of NEB; dashed line, basement membrane. (B) Ascl1 (green) is expressed during migration (left panels; E13) but downregulated during differentiation (right panels; E18), whereas CGRP (magenta) is detected only during differentiation. (C) E-cadherin is expressed around entire plasma membrane during NE selection (Ascl1-positive (green) cell at E13; left panels), but is downregulated in class 3 and 4 intermediates (some of which are marked by ZsGreen in E15 *Ascl1*$^{CreER/+}$;*Rosa26*$^{ZsGreen/+}$ mouse induced with tamoxifen at E12.5) in developing NEB (dotted outline; center panels). E-cadherin is again detected in NE cells (CGRP-positive; green) of mature NEB (PN 2 month; right panels), although expression is excluded from apical cell surface and detected along lateral boundaries in at least some cells. Cells neighboring NEB (not shown) express higher levels of E-cadherin and have larger apical surface that excludes E-cadherin. Lam, laminin γ1 (magenta). (D) Before NE selection (E12; left panels) epithelial progenitors are uniformly polarized and tight junction protein ZO-1 (magenta) is detected at apical surface of each cell. ZO-1 is downregulated and undetected in intermediates (*Ascl1*$^{CreER/+}$;*Rosa26*$^{ZsGreen/+}$ mouse labeled as above) during migration (center panels), when surrounding epithelial cells maintain its expression (inset), but is again detected during differentiation (right panels). (E) Snail proteins (magenta) are detected in some (filled arrowhead) but not other (open arrowhead) early NE progenitors (Ascl1-positive, green) during NE selection (E13; left panels), but all intermediates express Snail during migration (middle panels). Intermediates downregulate Snail in concert with Ascl1 as clusters form and differentiate (E15; right panels), as seen by declining level of Snail and Ascl1 in some cells (asterisks) within maturing cluster. Snail proteins are induced again later in NE cells (C.S.K., M.A.K., and J. Ouadah, unpublished data). Scale bar (B–F), 10 μm.

surrounding non-NE epithelial cells. Immunostaining also showed induction of neural cell adhesion molecule (NCAM) during NEB formation. NCAM was expressed in class 5 intermediates (Figures 7A and S7B), implying a role in NEB assembly or cohesion.

Immunostaining for epithelial apicobasal polarity markers integrin β1, laminin γ1, and zona occludens-1 (ZO-1), and analysis of the apicobasal distribution of E-cadherin, showed that developing NE cells also undergo dynamic changes in polarity. Progenitors prior to NE cell selection (Figures 7D and S7A), and epithelial cells not selected (Figures S7C and S7D), show the expected apicobasal distribution of markers (Figure 7A). However, early NE progenitors (class 1 and 2) lose integrin β1 and ZO-1 expression, and E-cadherin is distributed around the entire plasma membrane; the only apparent residual polarity is contact with the laminin γ1-expressing basal lamina (Figure 7A). Migrating class 3 intermediates appear to have lost epithelial structure and polarity, with E-cadherin expression diminished as noted above and no contact with the basal lamina or only residual contact in local areas of low or undetectable laminin γ1 (Figures 7C, 7D, and S7A). Class 4 intermediates begin to reestablish epithelial structure with E-cadherin again detected surrounding the entire cell

and their thin cytoplasmic extensions converging and contacting laminin in the basal lamina, suggesting re-initiation of apicobasal polarity (Figures 7A and 7D). Class 5 intermediates show continued maturation of epithelial structure and polarity that is complete in at least some cells, as evidenced by an expanded site of contact with laminin and basal lamina, expression of integrin β1 (Figure S7A) along the entire basolateral surface, and expression of ZO-1 at the apical plasma membrane and exclusion of E-cadherin from this domain (Figures 7A and 7D).

These morphological and molecular changes show that NE progenitors undergo a transient epithelial-to-mesenchymal transition (EMT) during migration and NEB formation. Many EMT events are controlled by Snail proteins, zinc finger transcription factors that drive the switch (Mani et al., 2008; Strobl-Mazzulla and Bronner, 2012). Using an anti-Snail antiserum to detect Snail 1, 2, and 3, none was detected in the earliest NE progenitors or any other epithelial cells (Figures 7A and 7E). However, soon after initiation of Ascl1 expression, nuclear Snail was detected and expression continued throughout cluster formation, before declining in class 5 intermediates as NE clusters form and re-establish epithelial structure and Ascl1 levels decline. We conclude that early NE progenitors induce Snail expression and undergo EMT, although it is an unconventional EMT as progenitors remain associated with the epithelium and the process soon reverses as progenitors downregulate Snail and restore epithelial structure and polarity on reaching the target.

## DISCUSSION

We have shown that NEBs form from NE progenitors initially distributed apparently randomly in the bronchial epithelium but then resolve in 2 days into clusters of 20–30 NE cells at stereotyped, diametrically opposed positions at the base of each bronchial branch. There is little or no progenitor proliferation during the process, so NEBs do not form by clonal expansion, as do *Drosophila* and other insect neurosensory organs. There is also little if any apoptosis of progenitors or reduction in progenitor number, so the clearing of progenitors from regions surrounding developing NEBs is not due to programmed cell death. Instead, lineage tracing, sparse labeling of progenitors, and high resolution imaging of intermediates in vivo, together with live imaging of progenitors in lung slices ex vivo, show that progenitors lose epithelial character and adopt fibroblast-like morphologies as they slowly (1–3 μm/hr for 1–2 days) crawl over and around neighboring epithelial cells, converging at diametrically opposed sites at the base of each bronchial branch and then rapidly (1–2 hr) joining the cluster. The intermediates express EMT transcription factor Snail and transiently downregulate E-cadherin and epithelial polarity proteins and then re-express these adhesion and polarity proteins and turn on NE differentiation genes and NCAM as they re-establish epithelial structure and assemble into a neurosensory organ.

The results lead us to propose that NEBs form by a targeted mode of epithelial cell sorting we call ''slithering,'' in which the rearranging cells transiently lose epithelial structure and polarity yet remain intimately associated with the epithelial sheet as they traverse neighboring epithelial cells and converge at the target site. This mechanism of cell rearrangement differs dramatically from intercalation, the classical mode of epithelial cell rearrangement, in which cells shrink lateral junctions with some neighboring cells while expanding junctions with others, exchanging positions while maintaining their polarized structure (Bertet et al., 2004; Blankenship et al., 2006; Guillot and Lecuit, 2013). At a mechanistic level, slithering is more reminiscent of cell delamination by EMT (Lamouille et al., 2014), such as during cancer metastasis (Scheel and Weinberg, 2012) or in neural crest formation where neural tube cells detach from the basement membrane and become mesenchyme-like cells that colonize distant sites (Strobl-Mazzulla and Bronner, 2012). During slithering, however, NE precursors never (or only transiently) leave the epithelial layer and they move comparatively short distances (tens of microns) and then rapidly regain epithelial character, so it is only a fleeting conversion. Epithelial cells can also undergo partial EMT during branching morphogenesis, in some organs forming highly dynamic, proliferative cell clusters at bud tips (Ewald et al., 2008), and individual proliferating epithelial cells can even occasionally send daughter cells to non-adjacent positions in the monolayer (''mitosis-associated cell dispersal'') (Packard et al., 2013). However, unlike these apparently random epithelial cell rearrangements and dispersals, slithering occurs without proliferation and is selective, directed, and purposeful. It results in active sorting of NE cells from surrounding epithelial cells in the monolayer, contrasting with the passive mechanisms long envisioned for cell sorting (Krens and Heisenberg, 2011; Steinberg, 1963) and forming neurosensory organs at defined positions.

Two prominent features of slithering are its selectivity for NE cells and their specific targeting to diametrically opposed positions at the base of each bronchial branch, raising the questions: what provides the guidance cue and its selectivity for NE cells? Because of the dynamic exploratory behavior of NE cells during slithering, we favor the idea that the guidance cue is a chemoattractant. Because only NE cells slither and they do so after turning on the master transcription factor Ascl1, we suggest that the chemoattractant receptor is specific for NE cells and part of their developmental program. However, there is no obvious cell or structure at target sites that could provide a point source of chemoattractant, and neurites that innervate NEBs arrive at their target only after the clusters form (Figures 2F and S3G–S3I). Perhaps the cue is a combination of more broadly distributed but overlapping signals, or even a physical signal related to the target structure: NEBs form at the most proximal and distal positions of the branch junction, where the connecting branches form the most obtuse (proximal) and acute (distal) angles. Although we have not systematically studied the formation of mini-clusters, available data indicate that they, too, form by slithering. However, because they do not form at stereotyped positions, their clustering could be driven by a homotypic attraction signal. A homotypic signal may also contribute to NEB formation, as real time imaging showed repeated transient contacts (''cell kisses'') among progenitors entering a NEB. A high priority now is to identify the signal(s) and their sources and receptors that control slithering and to determine if the same signals also guide outgrowth of neurites that target NEBs.

Because of the similarity in their developmental origins and clustered structures, slithering may also be used to form other

epithelial neurosensory organs such as taste buds (Chai et al., 2000; Okubo et al., 2009) and Merkel touch domes in skin that mediate light touch and spatial discrimination (Morrison et al., 2009; Van Keymeulen et al., 2009; Wright et al., 2015). Because slithering is difficult to detect without membrane marking or live imaging of individual intermediates, slithering could be a more widely used mechanism of movement and sorting of epithelial cells that has been overlooked even in well-studied epithelia such as the intestinal crypt, where Paneth cells move down from the proliferative zone as other cells move up (Batlle et al., 2002). Slithering appears to be a late evolutionary innovation, at least in the lung, because although all mammals studied have NEBs, the most primitive extant fish species have only solitary pulmonary NE cells (Zaccone et al., 1989).

It will be important to identify the slithering program and indeed the full program of NEB formation including cell selection, migration, differentiation, and innervation, and how these processes go awry in Notch pathway mutants (Morimoto et al., 2012; Tsao et al., 2009) and other forms of pulmonary NE cell disease including those with excess or misplaced NE cells (Nassar et al., 2011; Young et al., 2011). One appealing idea is that the slithering program is transiently reactivated in their stem cell function as they move out of their niche to replace dying neighboring cells and permanently activated by mutation during oncogenesis. The latter could explain why small cell lung cancer arising from pulmonary NE cells metastasize early and are the most deadly form of lung cancer.

## EXPERIMENTAL PROCEDURES

### Animals

CD-1 was wild-type strain. Cre alleles and reporters are described in the Supplemental Experimental Procedures. All animals were maintained and experiments performed in accordance with Stanford University's IACUC-approved protocols.

### Immunohistochemistry and Histology

Embryos and lungs from timed pregnancies, with noon of the day of vaginal plug detection designated E0.5, were dissected, fixed in paraformaldehyde (PFA), and immunostains of whole mount lungs performed as described (Metzger et al., 2008) except as noted (Supplemental Experimental Procedures), then imaged by confocal microscopy or optical projection tomography. For cryosections, tissue was fixed in PFA or Zamboni's fixative, cryoprotected in 30% sucrose, frozen in OCT, and stored at −80°C. Frozen tissue blocks were sectioned and incubated sequentially with blocking solution, primary antibody, secondary antibody conjugated to Alexa fluorophores, and DAPI. For full description of antibodies and methods, see the Supplemental Experimental Procedures.

### Mapping Pulmonary NE Cells

Serial sections of entire left lobes (n = 5) of E16 CD-1 mice were stained for E-cadherin and Ascl1 and branches L.L1, L.L2, L.L3, L.L4, L.D1, L.D2, L.D3, and L.D4 systematically examined for NE cells. Additional ages and branch points in left and right lung lobes were analyzed as described (Supplemental Experimental Procedures).

### Developmental Analysis of NE Cells

Serial sections of entire left lung lobes (n = 5 for each stage examined) of E12–E16 CD-1 mice were stained for Ascl1 and E-cadherin, and positions of NE cells were determined in branches and at junctions indicated. For NE cell counts (Figure S3D), serial sections of the entire left lobe were immunostained for Ascl1 and E-cadherin and cells scored in each segment along left main bronchus as indicated.

For EdU incorporation, 300 μg EdU was injected intraperitoneally and lungs harvested 2 hr later. EdU was detected by click chemistry in cryosections immunostained for Ascl1 and counterstained with DAPI, then visualized by confocal microscopy. For phospho-histone H3 analysis, cryosections were immunostained for Ascl1 and anti-phospho-Histone 3-Ser10.

### Lineage Tracing and Clonal Analysis

Lineage tracing was done with $Shh^{Cre/+;}Rosa26^{mTmG/+}$ mice (airway epithelial lineage) and with *Wnt1-Cre;*$Rosa26^{Zsgreen/+}$ (neural crest lineage). Lungs were harvested between E17.5– E18.5, fixed, cryosectioned, and immunostained as above. To test monoclonality of NEBs (Figure 3A), cryosectioned E18 $Shh^{Cre/+};Rosa26^{Rbw/+}$ lungs, in which all airway epithelial cells are permanently labeled early in development with one of the three Rainbow fluorescent reporters, were immunostained with anti-CGRP and an Alexa633-conjugated secondary. Cell number and colors in each NE cluster were assessed by confocal fluorescence microscopy. For clonal analysis, individual NE progenitors were sparsely labeled by tamoxifen injection at E11.5 (4 mg tamoxifen) or E12.5 (3 or 4 mg) of $Ascl1^{CreER/+};Rosa26^{Rbw\ /+}$ mice, and lungs were harvested between E17.5–E18.5 and analyzed as above.

### Labeling NE Developmental Intermediates

$Ascl1^{CreER/+};Rosa26^{ZsGreen/+}$ mice were induced with tamoxifen at E12.5, and lungs were harvested at E14.5 or E15.5 and serially sectioned, then co-stained for PGP9.5, E-cadherin and, for some samples, laminin gamma1 (γ1). NEBs and mini-clusters were analyzed by confocal microscopy, and a 35–40 μm z stack was collected and each labeled NE progenitor examined at high resolution. Three-dimensional reconstructions (Volocity) of each progenitor were used to identify cell shape, cytoplasmic processes, and interactions with other cells and basement membrane. Detailed descriptions of the morphologic classes are given in the Supplemental Experimental Procedures.

### Live Imaging of NE Cells in Slice Culture

$Ascl1^{CreER/+};Rosa26^{ZsGreen/mTmG}$ mice were induced with tamoxifen by oral gavage at E13 to label pulmonary NE progenitors with ZsGreen and mGFP and all other cells with TdTomato. At E15, lungs were harvested and left lobes and right caudal lobes separated, embedded in agarose and sectioned (Compresstome). Individual slices (175-μm thick) were transferred to a coverglass chamber, covered with Matrigel, and cultured in DMEM +F12 medium with 10% fetal bovine serum in an environmental chamber at 37°C and 5% $CO_2$. After 2–3 hr to establish the culture, confocal images were collected every 20 min for 60 hr. See the Supplemental Experimental Procedures.

## SUPPLEMENTAL INFORMATION

Supplemental Information includes Supplemental Experimental Procedures, seven figures, three tables, and two movies and can be found with this article online at http://dx.doi.org/10.1016/j.cell.2015.09.021.

## AUTHOR CONTRIBUTIONS

C.S.K. and M.A.K. conceived project and designed experiments. C.S.K. executed and analyzed experiments. C.S.K. and M.A.K. interpreted data and wrote the manuscript.

## ACKNOWLEDGMENTS

We thank Makenna Morck for help with slice culture experiments, Jozeph Pendleton for help with mouse colony maintenance, Dr. Andrew Olson (Stanford Neuroscience Microscopy Service, NIH NS069375) for advice on video processing, Dr. Jane Johnson for $Ascl1^{CreER}$ mice, members of the M.A.K. lab for discussions and comments on the manuscript, and Maria Petersen for help preparing the manuscript and figures. This work was supported by a grant from the NHLBI Progenitor Cell Biology Consortium (5U01HL099995), and a Tashia and John Morgridge Endowed Fellowship in Pediatric Translational

Medicine from the Stanford Child Health Research Institute (C.S.K.), Parker B. Francis Foundation Fellowship (C.S.K.), and NIH NHLBI K12 Scholar Award (C.S.K.). M.A.K. is an investigator of the Howard Hughes Medical Institute.

Received: April 13, 2015
Revised: July 8, 2015
Accepted: August 11, 2015
Published: October 1, 2015

## REFERENCES

Aguayo, S.M., Miller, Y.E., Waldron, J.A.J., Jr., Bogin, R.M., Sunday, M.E., Staton, G.W.J., Jr., Beam, W.R., and King, T.E.J., Jr. (1992). Brief report: idiopathic diffuse hyperplasia of pulmonary neuroendocrine cells and airways disease. N. Engl. J. Med. *327*, 1285–1288.

Aigouy, B., Farhadifar, R., Staple, D.B., Sagner, A., Röper, J.-C., Jülicher, F., and Eaton, S. (2010). Cell flow reorients the axis of planar polarity in the wing epithelium of Drosophila. Cell *142*, 773–786.

Anderson, D.J., and Axel, R. (1986). A bipotential neuroendocrine precursor whose choice of cell fate is determined by NGF and glucocorticoids. Cell *47*, 1079–1090.

Batlle, E., Henderson, J.T., Beghtel, H., van den Born, M.M.W., Sancho, E., Huls, G., Meeldijk, J., Robertson, J., van de Wetering, M., Pawson, T., and Clevers, H. (2002). Beta-catenin and TCF mediate cell positioning in the intestinal epithelium by controlling the expression of EphB/ephrinB. Cell *111*, 251–263.

Bertet, C., Sulak, L., and Lecuit, T. (2004). Myosin-dependent junction remodelling controls planar cell intercalation and axis elongation. Nature *429*, 667–671.

Blankenship, J.T., Backovic, S.T., Sanny, J.S.P., Weitz, O., and Zallen, J.A. (2006). Multicellular rosette formation links planar cell polarity to tissue morphogenesis. Dev. Cell *11*, 459–470.

Brouns, I., Oztay, F., Pintelon, I., De Proost, I., Lembrechts, R., Timmermans, J.-P., and Adriaensen, D. (2009). Neurochemical pattern of the complex innervation of neuroepithelial bodies in mouse lungs. Histochem. Cell Biol. *131*, 55–74.

Chai, Y., Jiang, X., Ito, Y., Bringas, P., Jr., Han, J., Rowitch, D.H., Soriano, P., McMahon, A.P., and Sucov, H.M. (2000). Fate of the mammalian cranial neural crest during tooth and mandibular morphogenesis. Development *127*, 1671–1679.

Cubas, P., de Celis, J.F., Campuzano, S., and Modolell, J. (1991). Proneural clusters of achaete-scute expression and the generation of sensory organs in the Drosophila imaginal wing disc. Genes Dev. *5*, 996–1008.

Cutz, E., Perrin, D.G., Pan, J., Haas, E.A., and Krous, H.F. (2007). Pulmonary neuroendocrine cells and neuroepithelial bodies in sudden infant death syndrome: potential markers of airway chemoreceptor dysfunction. Pediatr. Dev. Pathol. *10*, 106–116.

Cutz, E., Pan, J., Yeger, H., Domnik, N.J., and Fisher, J.T. (2013). Recent advances and contraversies on the role of pulmonary neuroepithelial bodies as airway sensors. Semin. Cell Dev. Biol. *24*, 40–50.

Deterding, R.R., Pye, C., Fan, L.L., and Langston, C. (2005). Persistent tachypnea of infancy is associated with neuroendocrine cell hyperplasia. Pediatr. Pulmonol. *40*, 157–165.

Ewald, A.J., Brenot, A., Duong, M., Chan, B.S., and Werb, Z. (2008). Collective epithelial migration and cell rearrangements drive mammary branching morphogenesis. Dev. Cell *14*, 570–581.

Feyrter, F. (1954). [Argyrophilia of bright cell system in bronchial tree in man]. Z. Mikrosk. Anat. Forsch. *61*, 73–81.

Gillan, J.E., and Cutz, E. (1993). Abnormal pulmonary bombesin immunoreactive cells in Wilson-Mikity syndrome (pulmonary dysmaturity) and bronchopulmonary dysplasia. Pediatr. Pathol. *13*, 165–180.

Gu, G., Dubauskaite, J., and Melton, D.A. (2002). Direct evidence for the pancreatic lineage: NGN3+ cells are islet progenitors and are distinct from duct progenitors. Development *129*, 2447–2457.

Guha, A., Vasconcelos, M., Cai, Y., Yoneda, M., Hinds, A., Qian, J., Li, G., Dickel, L., Johnson, J.E., Kimura, S., et al. (2012). Neuroepithelial body microenvironment is a niche for a distinct subset of Clara-like precursors in the developing airways. Proc. Natl. Acad. Sci. USA *109*, 12592–12597.

Guillot, C., and Lecuit, T. (2013). Mechanics of epithelial tissue homeostasis and morphogenesis. Science *340*, 1185–1189.

Harris, K.S., Zhang, Z., McManus, M.T., Harfe, B.D., and Sun, X. (2006). Dicer function is essential for lung epithelium morphogenesis. Proc. Natl. Acad. Sci. USA *103*, 2208–2213.

Irvine, K.D., and Wieschaus, E. (1994). Cell intercalation during Drosophila germband extension and its regulation by pair-rule segmentation genes. Development *120*, 827–841.

Ito, T., Udaka, N., Yazawa, T., Okudela, K., Hayashi, H., Sudo, T., Guillemot, F., Kageyama, R., and Kitamura, H. (2000). Basic helix-loop-helix transcription factors regulate the neuroendocrine differentiation of fetal mouse pulmonary epithelium. Development *127*, 3913–3921.

Kim, E.J., Ables, J.L., Dickel, L.K., Eisch, A.J., and Johnson, J.E. (2011). Ascl1 (Mash1) defines cells with long-term neurogenic potential in subgranular and subventricular zones in adult mouse brain. PLoS ONE *6*, e18472.

Krens, S.F.G., and Heisenberg, C.-P. (2011). Cell sorting in development. Curr. Top. Dev. Biol. *95*, 189–213.

Lamouille, S., Xu, J., and Derynck, R. (2014). Molecular mechanisms of epithelial-mesenchymal transition. Nat. Rev. Mol. Cell Biol. *15*, 178–196.

Lauweryns, J.M., and Peuskens, J.C. (1972). Neuro-epithelial bodies (neuroreceptor or secretory organs?) in human infant bronchial and bronchiolar epithelium. Anat. Rec. *172*, 471–481.

Lauweryns, J.M., and Van Lommel, A. (1987). Ultrastructure of nerve endings and synaptic junctions in rabbit intrapulmonary neuroepithelial bodies: a single and serial section analysis. J. Anat. *151*, 65–83.

Lawrence, P.A. (1966). Development and determination of hairs and bristles in the milkweed bug, Oncopeltus fasciatus (Lygaeidae, Hemiptera). J. Cell Sci. *1*, 475–498.

Mani, S.A., Guo, W., Liao, M.-J., Eaton, E.N., Ayyanan, A., Zhou, A.Y., Brooks, M., Reinhard, F., Zhang, C.C., Shipitsin, M., et al. (2008). The epithelial-mesenchymal transition generates cells with properties of stem cells. Cell *133*, 704–715.

Metzger, R.J., Klein, O.D., Martin, G.R., and Krasnow, M.A. (2008). The branching programme of mouse lung development. Nature *453*, 745–750.

Morimoto, M., Nishinakamura, R., Saga, Y., and Kopan, R. (2012). Different assemblies of Notch receptors coordinate the distribution of the major bronchial Clara, ciliated and neuroendocrine cells. Development *139*, 4365–4373.

Morrison, K.M., Miesegaes, G.R., Lumpkin, E.A., and Maricich, S.M. (2009). Mammalian Merkel cells are descended from the epidermal lineage. Dev. Biol. *336*, 76–83.

Nassar, A.A., Jaroszewski, D.E., Helmers, R.A., Colby, T.V., Patel, B.M., and Mookadam, F. (2011). Diffuse idiopathic pulmonary neuroendocrine cell hyperplasia: a systematic overview. Am. J. Respir. Crit. Care Med. *184*, 8–16.

Okubo, T., Clark, C., and Hogan, B.L.M. (2009). Cell lineage mapping of taste bud cells and keratinocytes in the mouse tongue and soft palate. Stem Cells *27*, 442–450.

Packard, A., Georgas, K., Michos, O., Riccio, P., Cebrian, C., Combes, A.N., Ju, A., Ferrer-Vaquer, A., Hadjantonakis, A.-K., Zong, H., et al. (2013). Luminal mitosis drives epithelial cell dispersal within the branching ureteric bud. Dev. Cell *27*, 319–330.

Park, K.-S., Liang, M.-C., Raiser, D.M., Zamponi, R., Roach, R.R., Curtis, S.J., Walton, Z., Schaffer, B.E., Roake, C.M., Zmoos, A.-F., et al. (2011). Characterization of the cell of origin for small cell lung cancer. Cell Cycle *10*, 2806–2815.

Polak, J.M., Becker, K.L., Cutz, E., Gail, D.B., Goniakowska-Witalinska, L., Gosney, J.R., Lauweryns, J.M., Linnoila, I., McDowell, E.M., Miller, Y.E., et al. (1993). Lung endocrine cell markers, peptides, and amines. Anat. Rec. *236*, 169–171.

Reynolds, S.D., Hong, K.U., Giangreco, A., Mango, G.W., Guron, C., Morimoto, Y., and Stripp, B.R. (2000). Conditional clara cell ablation reveals a self-renewing progenitor function of pulmonary neuroendocrine cells. Am. J. Physiol. Lung Cell. Mol. Physiol. *278*, L1256–L1263.

Rinkevich, Y., Lindau, P., Ueno, H., Longaker, M.T., and Weissman, I.L. (2011). Germ-layer and lineage-restricted stem/progenitors regenerate the mouse digit tip. Nature *476*, 409–413.

Rock, J.R., and Hogan, B.L.M. (2011). Epithelial progenitor cells in lung development, maintenance, repair, and disease. Annu. Rev. Cell Dev. Biol. *27*, 493–512.

Scheel, C., and Weinberg, R.A. (2012). Cancer stem cells and epithelial-mesenchymal transition: concepts and molecular links. Semin. Cancer Biol. *22*, 396–403.

Scheuermann, D.W. (1987). Morphology and cytochemistry of the endocrine epithelial system in the lung. Int. Rev. Cytol. *106*, 35–88.

Song, H., Yao, E., Lin, C., Gacayan, R., Chen, M.-H., and Chuang, P.-T. (2012). Functional characterization of pulmonary neuroendocrine cells in lung development, injury, and tumorigenesis. Proc. Natl. Acad. Sci. USA *109*, 17531–17536.

Steinberg, M.S. (1963). Reconstruction of tissues by dissociated cells. Some morphogenetic tissue movements and the sorting out of embryonic cells may have a common explanation. Science *141*, 401–408.

Strobl-Mazzulla, P.H., and Bronner, M.E. (2012). Epithelial to mesenchymal transition: new and old insights from the classical neural crest model. Semin. Cancer Biol. *22*, 411–416.

Sutherland, K.D., Proost, N., Brouns, I., Adriaensen, D., Song, J.-Y., and Berns, A. (2011). Cell of origin of small cell lung cancer: inactivation of Trp53 and Rb1 in distinct cell types of adult mouse lung. Cancer Cell *19*, 754–764.

Tsao, P.-N., Vasconcelos, M., Izvolsky, K.I., Qian, J., Lu, J., and Cardoso, W.V. (2009). Notch signaling controls the balance of ciliated and secretory cell fates in developing airways. Development *136*, 2297–2307.

Van Keymeulen, A., Mascre, G., Youseff, K.K., Harel, I., Michaux, C., De Geest, N., Szpalski, C., Achouri, Y., Bloch, W., Hassan, B.A., and Blanpain, C. (2009). Epidermal progenitors give rise to Merkel cells during embryonic development and adult homeostasis. J. Cell Biol. *187*, 91–100.

van Meerbeeck, J.P., Fennell, D.A., and De Ruysscher, D.K.M. (2011). Small-cell lung cancer. Lancet *378*, 1741–1755.

Wright, M.C., Reed-Geaghan, E.G., Bolock, A.M., Fujiyama, T., Hoshino, M., and Maricich, S.M. (2015). Unipotent, Atoh1+ progenitors maintain the Merkel cell population in embryonic and adult mice. J. Cell Biol. *208*, 367–379.

Young, L.R., Brody, A.S., Inge, T.H., Acton, J.D., Bokulic, R.E., Langston, C., and Deutsch, G.H. (2011). Neuroendocrine cell distribution and frequency distinguish neuroendocrine cell hyperplasia of infancy from other pulmonary disorders. Chest *139*, 1060–1071.

Zaccone, G., Tagliafierro, G., Goniakowska-Witalinska, L., Fasulo, S., Ainis, L., and Mauceri, A. (1989). Serotonin-like immunoreactive cells in the pulmonary epithelium of ancient fish species. Histochemistry *92*, 61–63.

Cell

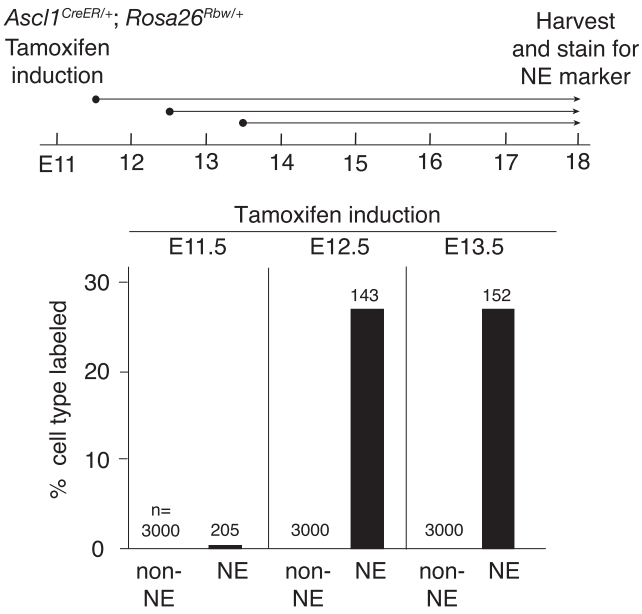


**Figure S1. Temporal Profile and Cell Specificity of *Ascl1*$^{CreER}$ Lineage Trace, Related to Experimental Procedures**

Top: experimental scheme. Tamoxifen (4 mg) was injected into *Ascl1*$^{CreER/+}$;*Rosa26*$^{Rbw/+}$ mice at the times indicated (circles) to induce Cre recombination and lineage label *Ascl1*-expressing cells. Lungs were harvested at E18, sectioned, and lineage-labeled cells analyzed by co-staining for the mature NE markers CGRP or PGP9.5. Bottom: quantification showing fraction of E18 neuroendocrine cells (CGRP- or PGP9.5-positive) or non-NE cells (CGRP- or PGP9.5-negative) airway epithelial cells expressing the lineage trace when induced at the embryonic ages indicated. n, number of scored cells from 2 different lungs. *Ascl1*$^{CreER}$ shows lineage trace activity beginning at E11.5 and labels exclusively NE cell progenitors.

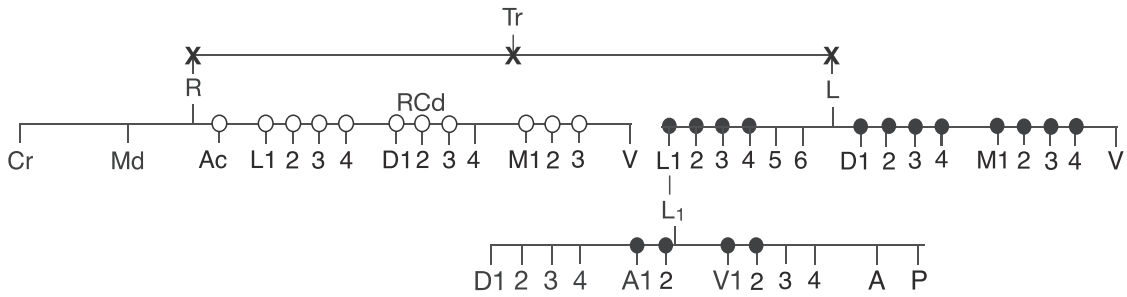


**Figure S2. Mapped NEBs in the Mouse Branch Lineage, Related to Figure 1**

A portion of the branch lineage of the mouse bronchial tree is shown, with the positions of NEBs systematically mapped (n = 5 lungs) in the left lobe at E16-E18 indicated by filled circles. NEBs were found exclusively at branch junctions, and each junction scored (except those indicated by an X) contained a pair of diametrically-opposed NEBs oriented along the proximal to distal axis. The same results were obtained at randomly-selected junctions scored (open circles; n = 70 junctions in 5 lungs) in the right caudal (RCd) and accessory (Ac) lobes and many other junctions throughout the lung (not shown).

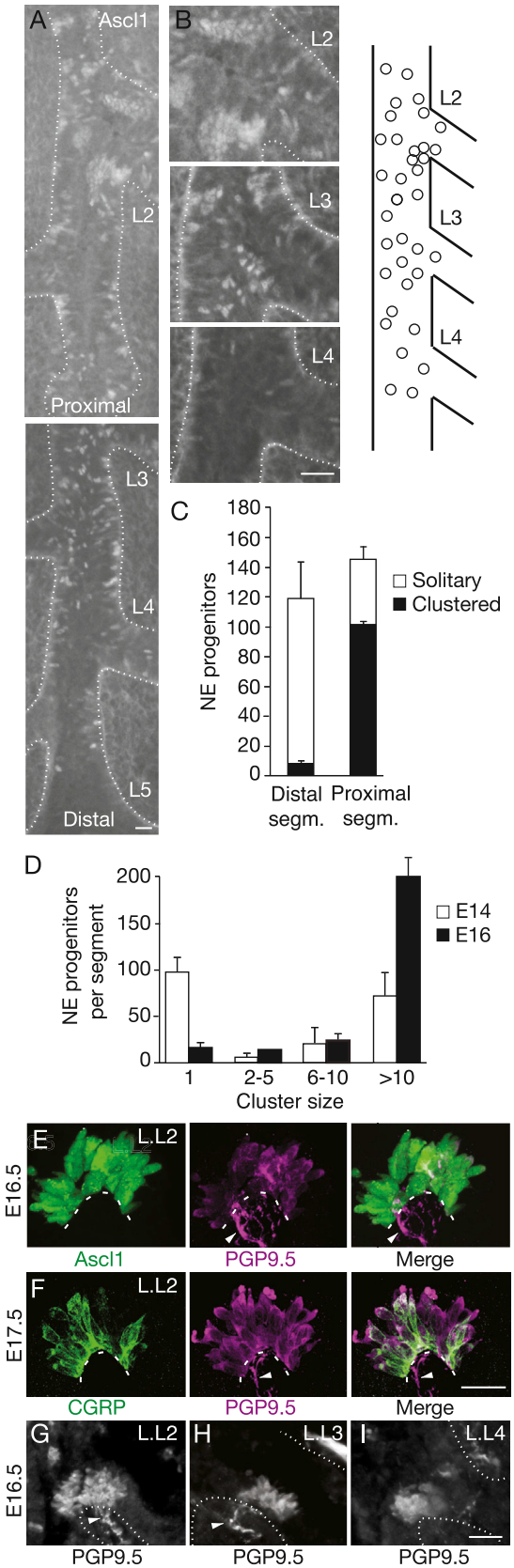


*(legend on next page)*

**Figure S3. NEB Development Initiates in a Proximal to Distal Temporal Sequence, Related to Figure 2**

(A) A montage of longitudinal sections through the left primary bronchus in E14 wild-type CD-1 lung immunostained for Ascl1 to show NE progenitors. Note multiple stages of NEB development are detected along proximal-distal axis, with progenitor selection not yet begun at L.L5, recently initiated at L.L4, and cluster formation begun at L.L3 and advanced at L.L2.

(B) Close-up of L.L2, L.L3, and L.L4 branchpoints in A showing large cluster at L.L2, small nascent clusters at L.L3, and only solitary cells at L.L4, as schematized at right.

(C) Quantification of NE progenitor clustering by position. Values shown are the number of solitary (open) and clustered (filled) NE cells (mean ± SEM; bars at top show SEM for total cells; n = 3 lungs) in proximal (base of L.L1 through base of L.L2) and distal (base of L.L4 through L.L5) segments of a continuous image plane along left primary bronchus (L). Note similar number of cells in the segments but more clustering in the proximal segment.

(D) Histogram showing distribution of NE cells among different size NE clusters at E14 (open bars; mean ± SEM; n = 4 lungs) and E16 (filled bars; n = 3 lungs) in one complete distal segment (base of L.L4 through base of L.L5) of left primary bronchus. Note shift in distribution toward larger clusters from E14 to E16.

(E–I) Spatiotemporal analysis of PGP9.5 expression during NEB development. (E) Confocal image of L.L2d NEB in E16.5 *Ascl1*$^{CreER/+}$; *Rosa26*$^{ZsGreen/+}$ mouse induced at E13 with tamoxifen to label NE cells with ZsGreen (Ascl1 lineage, green) and immunostained for PGP9.5 (magenta). PGP9.5 expression has initiated in many of the NEB cells. PGP9.5-expressing nerve fibers (arrowhead) have grown toward and begun ramifying on NEB cells. (F) L.L2d NEB as above in E17.5 wild-type mouse immunostained for CGRP (green) and PGP9.5 (magenta). PGP9.5 is expressed robustly in all the NEB cells, and CGRP has initiated expression in some of them. (G–I) PGP9.5 expression as in E in L.L2d (G), L.L3d (H), and L.L4d (I) NEBs along left main bronchus of E16.5 wild-type mouse immunostained with PGP9.5 (white). PGP9.5 expression has initiated at all three positions and innervation (arrowheads) has begun at L.L2 and L.L3 NEBs but not L.L4 NEB. Scale bars, 50 μm (A, B, G-I), 10 μm (E, F).

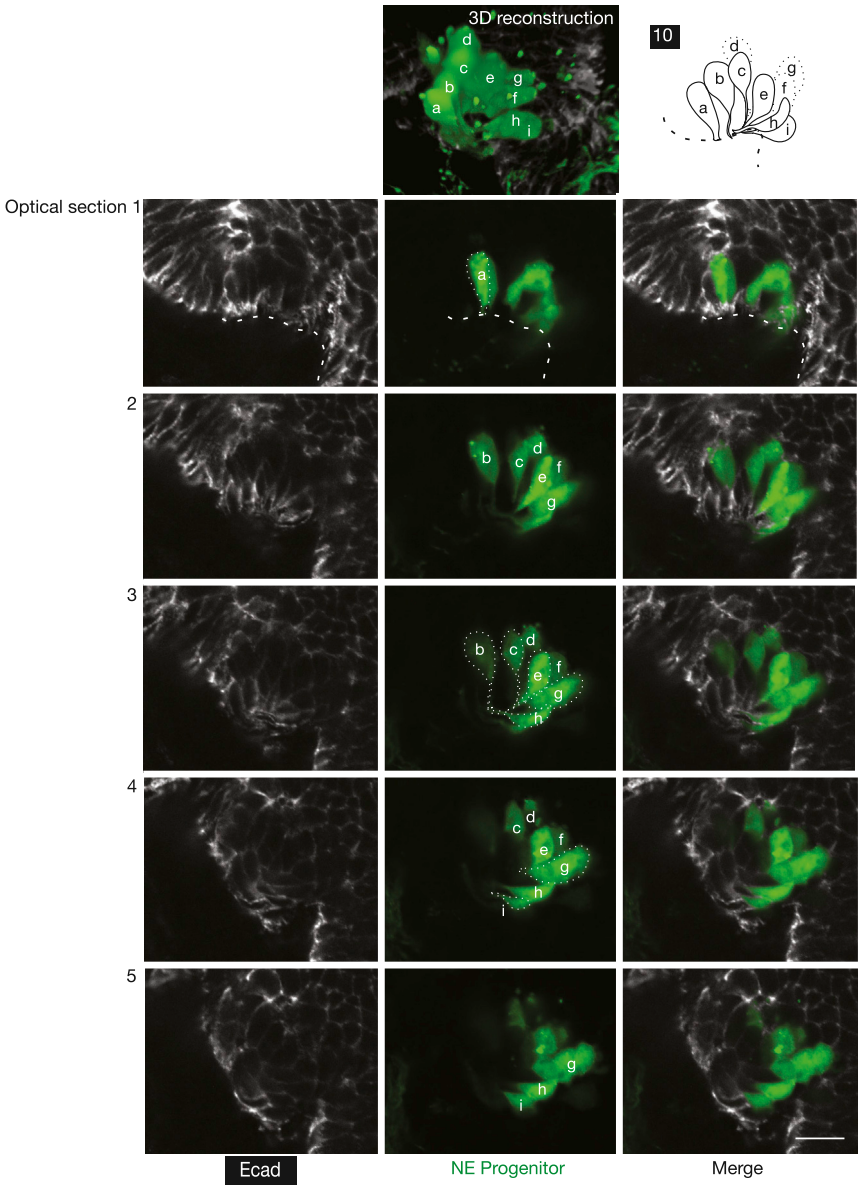


**Figure S4. Example of 3D Reconstruction of Cellular Intermediates at a Developing NEB, Related to Figure 5 and Table S3**

Optical sections and schematic of intermediates at a developing NEB (cluster 10 in Table S3). Micrographs show 3D reconstruction with schematic (row 1) and serial optical sections (confocal stack, 1 μm z-dimension) through a developing NEB in an *Ascl1*$^{CreER/+}$;*Rosa26*$^{ZsGreen/+}$ mouse induced with tamoxifen at E12.5 to label NE progenitors (green) and harvested 48 hr later and co-stained for E-cadherin (white) to outline epithelial cells. Volocity software was used to determine overall structure and orientation of intermediates and construct a 3D rendering of cells for the schematic, and then individual sections were carefully examined to ascertain precise cell morphologies and boundaries in the 3D reconstruction and assign intermediate class. Each labeled intermediate is designated by a letter in the micrographs and schematics, and its class assignment is indicated in Table S3 by its fill color according to the scheme shown. Black, outlines of complete individual NE cells; dots, outlines of individual NE cells that extend beyond the imaged region; dashed line, basement membrane. Scale bar, 10 μm.

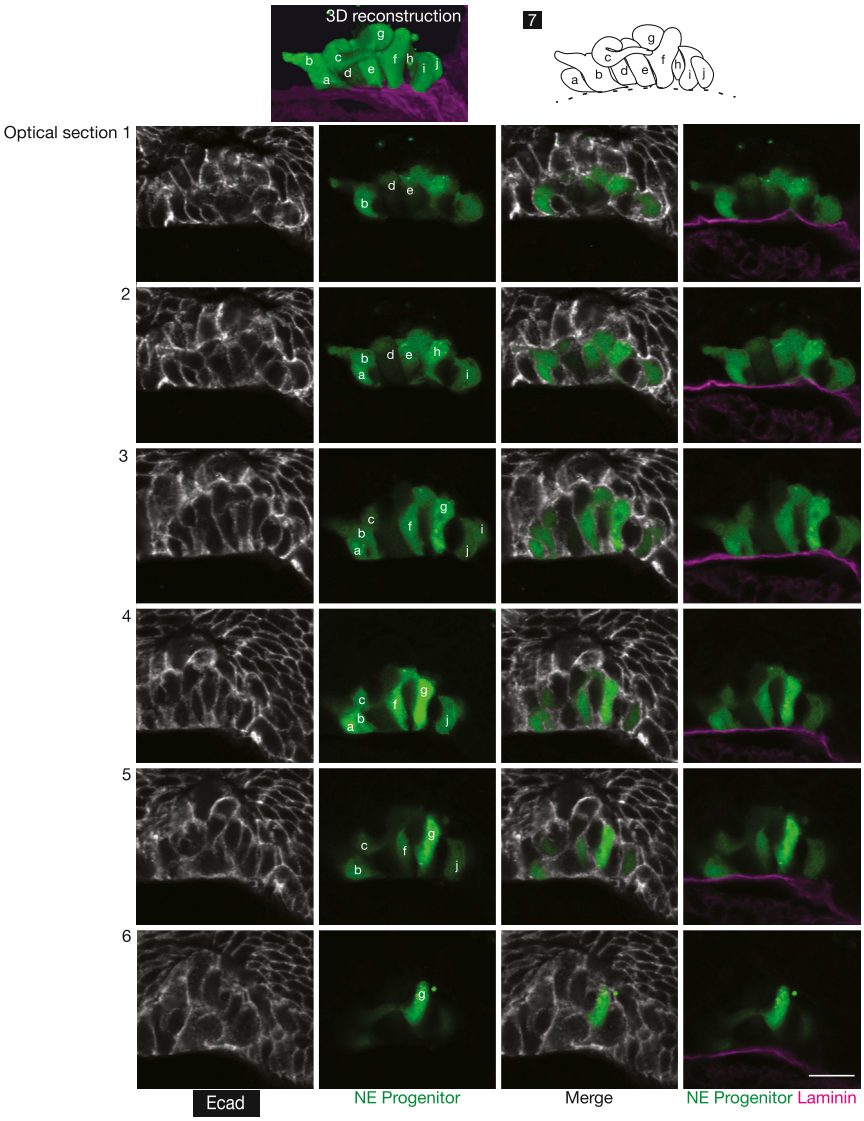


**Figure S5. Second Example of 3D Reconstruction of Cellular Intermediates at a Developing NEB, Related to Figure 5 and Table S3**
Optical sections and schematic of intermediates at a developing NEB (cluster 7 in Table S3) as in Figure S4. Scale bar, 10 μm.

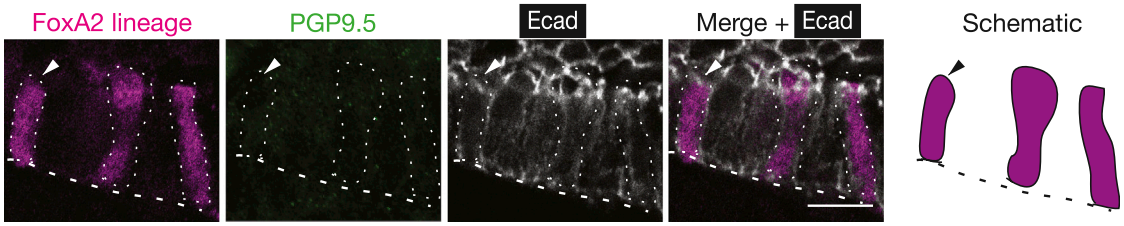


**Figure S6. Morphology of Bronchial Epithelial Cells during NEB Formation, Related to Figure 5**

Confocal images of typical bronchial epithelial cells in a cryosectioned E15 lung from *FoxA2*$^{CreER/+}$; *Rosa26*$^{TdTomato/+}$ induced with 2.5 mg tamoxifen at E9.0 to randomly label airway epithelial cells (magenta) and immunostained for E-cadherin (white) and PGP9.5 (green) to detect NE cells. Nearly all (> 90%) of PGP9.5-negative cells (n = 300) had standard pseudostratified columnar epithelial cell structure like the three FoxA2 lineage-labeled cells shown (dotted outlines), with each cell contacting the basement membrane (dashed line) and extending to the airway lumen (arrowhead). In contrast, ~30% of PGP9.5-positive cells and associated cells (n = 50) at sites of forming NEBs (not shown) had distinct morphologies, like class 2, 3 and 4 NE intermediates (see Figure 5). Scale bar, 10 μm.

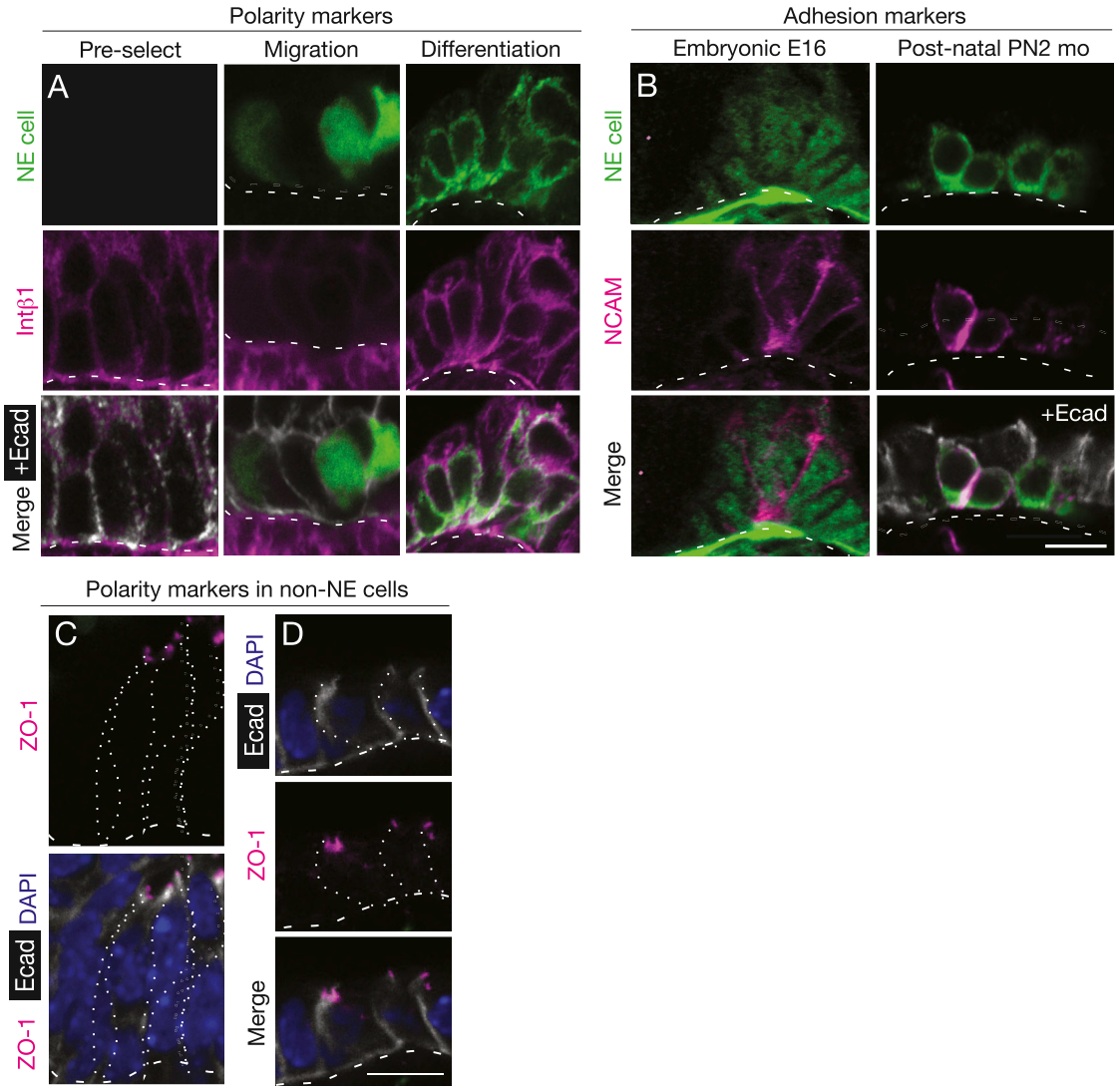


**Figure S7. Changes in Adhesion and Polarization of NE Cells during Development, Related to Figure 7**

(A) Confocal images of lungs showing NEB progenitors before NE cell selection (E12, Pre-select), during NE migration (E15, Migration), and during NE differentiation (E18) immunostained for integrin β1 (magenta), E-cadherin (white), and a NE marker (*Ascl1*$^{CreER/+}$;*Rosa26*$^{ZsGreen/+}$ sparse labeling in Migration; CGRP immunostain in Differentiation). Note integrin β1 is detected in a basolateral distribution (similar to E-cadherin) before specification, is downregulated in migrating intermediates, and is again detected in a basolateral distribution in maturing cells in the NEB during differentiation.

(B) Confocal section of a developing NEB at E16 (left) and a mature NEB in an adult (postnatal 2 months) immunostained for neural cell adhesion molecule (NCAM, magenta) and a NE marker (Ascl1 left; CGRP right). Neural cell adhesion molecule (NCAM) begins to be expressed in NE cells upon cluster formation (E16, left) and continues in the adult (right), although some NE cells in the mature NEB express it more strongly than others.

(C and D) Expression of polarity marker zona occludens 1 (ZO-1) in non-NE cells of developing bronchial epithelium. Confocal images of proximal (C) and distal (D) airway epithelium in E15 lung sections from *Ascl1*$^{CreER/+}$;*Rosa26*$^{ZsGreen/+}$ mice induced at E12.5 with tamoxifen and immunostained for the apical tight junction marker zona occludens 1 (ZO-1; magenta), E-cadherin (white) and DAPI (blue) as indicated. Regions of the epithelium shown are adjacent to the regions containing labeled NE intermediates in Figure 7D. Note that in both the pseudostratified proximal epithelium (C) and cuboidal distal epithelium (D), ZO-1 localizes to a thin band at the apical lateral surface, demonstrating apicobasal polarity of the cells. This contrasts with migrating NE progenitors in adjacent regions (Figure 7D), in which ZO-1 is not detected and apicobasal polarity is apparently lost. Scale bars in B (for A, B) and D (for C, D), 10 μm.

**Cell**

**Supplemental Information**

# Formation of a Neurosensory Organ by Epithelial Cell Slithering

**Christin S. Kuo and Mark A. Krasnow**

**Supplemental Experimental Procedures**

**Animals**

CD-1 (Charles Rivers Labs) was the wild type strain; it was always used for developmental analysis because there can be strain differences in developmental timing. Other strains used were: Cre recombinase knock-in alleles *Ascl1CreERT2* (Kim et al., 2011) (abbreviated here *"Ascl1$^{CreER}$"), Shh$^{Cre}$* (Jackson Labs B6.Cg-$^{Shh\ tm1(EGFP/cre)Cjt}$/J) (Harfe et al., 2004), and *FoxA2$^{mcm}$* (Park et al., 2007) (Jackson Labs *Foxa2$^{tm2.1(cre/Esr1*)Moon}$/J, "FoxA2$^{CreER}$"); Cre*-expressing transgenic line *Wnt1-Cre* (Danielian et al., 1998) and Cre-dependent reporters *Rosa26$^{mTmG}$* , *Rosa26$^{ZsGreen}$*, and *Rosa26$^{Rainbow}$ ("Rosa26$^{Rbw}$")* (Madisen et al., 2010; Muzumdar et al., 2007; Rinkevich et al., 2011).

**Immunohistochemistry and histology**

Embryos and lungs from timed pregnancies, with noon of the day of vaginal plug detection designated E0.5, were dissected and fixed in 4% paraformaldehyde (PFA) for 0.5-2 hr. Immunostains of whole mount lungs were performed as described (Metzger et al., 2008) with the modifications noted below. Fixed lungs were dehydrated serially into 100% methanol and stored at -20°C. Lungs were rehydrated and incubated with blocking solution (5% goat serum, 0.5% Triton X-100 in PBS) and then with primary antibodies diluted in blocking solution for 48-72 hours at 4°C. On the next day, lungs were washed with blocking solution, followed by incubation with fluorescent-conjugated secondary antibodies overnight at 4°C. For signal amplification, a biotin-conjugated antibody was used with ABC Elite reagent (Vector) followed by fluorescein (FITC) or Cy3 Tyramide Reagent (Perkin Elmer). Lungs were dehydrated and placed in benzyl alcohol:benzyl benzoate (1:2) solution (BABB) prior to imaging by either laser scanning confocal fluorescence microscopy (Leica SP2 or Zeiss LSM 780) or optical projection tomography (OPT;Bioptonics 3001).

For immunostaining of lung sections, lungs were dissected and fixed in 4% PFA or Zamboni's fixative (American MasterTech Scientific, #FXZAMLT) for 0.5-2 hours and cryoprotected in 30% sucrose overnight at 4°C, frozen in optical cutting temperature compound (OCT, Tissue Tek) and stored at -80°C. Frozen tissue blocks were sectioned (20-50 μm) and the sections washed in 0.1% Tween-20 in PBS (PBST) and then incubated with blocking solution (5% goat serum, 0.3% Triton X-100 in PBS) for 1-5 hrs, and washed in PBST. The washed sections were then incubated with primary antibodies overnight at 4$^{o}$C, washed with PBST, and then incubated with secondary antibodies at room temperature for 45 minutes, followed by staining with DAPI to mark nuclei.

Primary antibodies were: anti-Ascl1 (mouse, BD Pharmingen, 1:500), monoclonal anti-alpha smooth muscle actin (SMA)-Cy3, Sigma C6198, 1:250), anti-CGRP (rabbit, BioMol, 1:500 - 1:1000; guinea pig, Europroxima, 1:500-1:1000), anti-cleaved caspase3 (rabbit, Cell-signaling, 1:200), anti-E-cadherin (rat, Invitrogen, 1:500; rabbit, Cell-signaling, 1:250), anti-integrin β1 (rat, Millipore, 1:200),

anti-laminin γ1 (rat, Millipore, 1:500), anti-NCAM (rabbit, Millipore, 1:500), anti-PGP9.5 (rabbit, Dako, 1:500), anti-ZO-1 (rabbit, Invitrogen, 1:200), and anti-Snail (rabbit, 1:500). The anti-Snail antiserum was raised against a peptide (RMSLLHKHQESGSSGGPR) (Rukstalis and Habener, 2007) with 95% sequence identity to the N-terminus of mouse Snail1, 68% to Snail2, and 63% to Snail3. Secondary antibodies were directly conjugated to Alexa -488, -555, or 633 (Invitrogen), or to Alexa 647 (donkey anti-rat, Jackson ImmunoResearch) and all used at 1:250 dilution.

**Mapping locations of pulmonary NE cells**

In addition to left lobe lateral branches (L.L1-L.L4 and L.D1-L.D4) (see Experimental Procedures), left lobe branches L.M1, L.M2, L.M3, L.M4, L.L1.A1, L.L1.A2, L.L1.V1, L.L1.V2 were analyzed in whole mount E18 CD-1 lungs co-stained for anti-alpha smooth muscle actin (bronchial branches) and CGRP (NE cells). The 3D bronchial branch lineage was easy to visualize in whole-mounts, however only positions of large NE clusters (NEBs) could be reliably scored at this resolution. Right lungs were similarly prepared and analyzed in the right caudal lobe (R.Cd.L1-4, R.Cd.D1-3, R.Cd.M1-3) and also at secondary branches in the accessory lobe, although this analysis was less systematic. In addition, E18 lungs from *Ascl1*$^{CreER/+}$*; Rosa26*$^{mTmG/+}$ mice injected with tamoxifen at E14 to label NE cells were sectioned (entire left lobes, 40-50 μm sections), immunostained for E-cadherin, and analyzed by confocal microscopy to identify NEBs at locations L.L1-4. All positions and mapping strategies gave similar results.

**Lineage labeling and clonal analysis of NE cell proliferation**

Lineage labeling to investigate the number of progenitors that contribute to NEBs was done using *Shh*$^{Cre/+}$;*Rosa26*$^{Rbw/+}$ embryos to label all epithelial cells with one of three fluorescent proteins early in lung development. Lungs were harvested at E18, fixed with 4% PFA as described above, cryosectioned (35 μm sections) and immunostained with rabbit anti-CGRP and secondary goat anti-rabbit Alexa 633. For each cluster or NEB, cell number and fluorescent colors were scored by confocal microscopy.

For clonal analysis, individual NE progenitors were sparsely labeled by intraperitoneal tamoxifen injection of *Ascl1*$^{CreER/+}$*;Rosa26*$^{Rbw/+}$ mice soon after Ascl1 expression initiates (E11.5; 4 mg tamoxifen) or a day later (E12.5; 3 or 4 mg tamoxifen). Embryos were harvested at E17.5, and lungs were dissected, embedded, and sectioned (35 μm) as above. Sections were immunostained for CGRP to identify NEBs, and the number of NE cells and expression of Rainbow reporters was determined by confocal fluorescence microscopy.

**EdU incorporation and phospho-histone analysis of NE cell proliferation**

Wild-type CD-1 timed pregnant females at embryonic stages E13.5, E14.5, E15.5, and E16.5 were injected intraperitoneally with 300 μg of the synthetic deoxyribonucleotide analogue EdU (5-ethynyl-2'-deoxyuridine; Invitrogen C10337). Two hours later, embryonic lungs were dissected, fixed,

and embedded, and the frozen blocks stored at -80°C until sectioning. Sections (20-30 μm thick) were immunostained for Ascl1 and detected with goat anti-mouse secondary antibody (A555). EdU signal was detected using click chemistry (A488, Invitrogen/Life Tech) according to manufacture's instructions, and nuclei were counterstained with DAPI (1 μg/ml). Specific bronchi were visualized by confocal microscopy and NE (Ascl1-positive) and non-NE (Ascl1-negative bronchial epithelial cells) were scored for EdU-positive nuclei. Lung sections stained for Ascl1 and cell proliferation marker phosphorylated histone 3 (anti-phospho-Histone 3-Ser10, rabbit, Millipore, 1:250) gave similar results, although the EdU protocol labeled more cells.

**Activated caspase-3 immunostaining of NE cell death**

Wild type CD-1 lungs were harvested during the period of NE clustering and local clearing of solitary NE progenitors (E14.5, E15.5, and E16.5), and fixed, embedded, sectioned, and immunostained for Ascl1 (secondary anti-mouse $IgG_1$ A555) and for activated Caspase-3 (rabbit anti-cleaved Caspase-3; secondary anti-rabbit A488) to detect dying cells, and nuclei were counterstained with DAPI. Confocal z-stacks were acquired along the bronchial epithelium, and all NE (Ascl1-positive) and non-NE cells (Ascl1-negative, DAPI-positive epithelial cells) within each z-stack (~30 μm thick) were scored for expression of cleaved Caspase-3. Scoring was done both at proximal and more distal positions to include regions with NE progenitors at different stages of development.

**Classifying NE cell developmental intermediates**

Intermediates were divided into 5 different structural classes, as follows: Class 1: Typical columnar or pseudostratified epithelial morphology without cellular protrusions or extensions and indistinguishable from neighboring non-NE bronchiolar epithelial cells. Class 2: Cells with multiple cellular extensions originating from apical or lateral plasma membrane and up to 30 μm in length. Class 3: Cells with irregular shapes (twisted, bent) and not aligned with neighboring epithelial cells, and no contact, or contact by just a thin projection, with laminin-positive basement membrane. Class 4: Cells with similar orientation as neighboring airway epithelial cells but with basal thin extensions swirling toward basement membrane with similar extensions from neighboring NE cell intermediates and converging at a common point along basement membrane. Class 5: Cells with normal apicobasal orientation and in cluster with other NE cells and fully contacting basement membrane. The only intermediates outside these five structural classes were ones oriented horizontally along the basement membrane (Table S3C, cell 16h) and rare “spiky” cells (Table S3C, cell 20b).

**Live imaging of NE cells in slice cultures**

*Ascl1*$^{CreER/+}$;*Rosa26*$^{ZsGreen/mTmG}$ mice were induced with 3 mg tamoxifen by oral gavage at E13 to label pulmonary NE cell intermediates with ZsGreen and membrane GFP. All other cells express TdTomato, which allows direct visualization of the epithelium and easy distinction of NE cells (ZsGreen

and mGFP-positive cells within the epithelium) from Ascl1-positive neurons (ZsGreen and mGFP-positive cells outside the epithelium). Lungs were harvested at E15 and left lobes and right caudal lobes were separated and embedded in 3% agarose and then sectioned with Compresstome (VF 200) to generate lung slices (175 μm thick). All dissection steps prior to placement in culturing chamber were performed in cold (4$^{o}$ C) PBS. Individual lung slices were transferred to an 8-well coverglass chamber (Lab-Tek #70378-82) and a drop of Matrigel (Corning #354230) was placed on top of the sample and incubated at 37$^{o}$C for 10 minutes to solidify. Culture media (DMEM +F12 and 10% fetal bovine serum) + penicillin-streptomycin (final concentration 100 μg/ml) was added and slices were returned to 37$^{o}$C for 2-3 hours to allow cultures to establish. Time lapse imaging (image acquisition every 20 minutes for over 60 hours) was performed using a Zeiss 780 confocal equipped with an environmental chamber to maintain the culture at 37$^{o}$C and 5% $CO_2$. Under these culture conditions, lung slices showed minimal cell death after 48 hours as assayed by SYTO10 staining (Dead Red kit #L7013, Invitrogen/Life Tech).

**Marker expression analysis of NE intermediates**

NE developmental intermediates in the lungs of *Ascl1*$^{CreER/+}$;*Rosa26*$^{ZsGreen/+}$ mice were labeled with ZsGreen and DAPI as described above and co-stained for E-cadherin and a NE, adhesion, or apical basal marker as indicated in the figures. Thinner sections (35 μm) were used for optimal immunostaining, which was especially important for detecting and analyzing ZO-1. For the all pre-NE specification and some of the differentiation stage samples, when all NE progenitors are of a single class, lungs from wild type CD-1 mice were used and immunostained for Ascl1 or CGRP to detect NE cells. NCAM staining was only detected in NE cells after cluster formation (class 5 intermediates).

**Table S1.** Multiple Lineage Contributions to Pulmonary NE Clusters, Related to Figure 3.

| NE cluster[1] | No. of NE cells[2] | Cherry cells[2] | Orange cells[2] | Cerulean cells[2] |
|---|---|---|---|---|
| 1 | 5 | 2 | 2 | 1 |
| 2 | 7 | 2 | 3 | 2 |
| 3 | 7 | 2 | 3 | 2 |
| 4 | 8 | 3 | 2 | 3 |
| 5 | 10 | 3 | 5 | 2 |
| 6 | 14 | 3 | 6 | 5 |
| 7 | 15 | 5 | 5 | 5 |
| 8 | 19 | 3 | 10 | 6 |
| 9 | 21 | 5 | 10 | 6 |
| 10 | 27 | 11 | 9 | 7 |
| 11 | 28 | 12 | 6 | 10 |
| 12 | 38 | 12 | 16 | 10 |

[1] NE clusters in *Shh*$^{Cre/+}$;*Rosa26*$^{Rbw/+}$ mice with airway epithelial progenitors stochastically labeled early in lung development with one of three fluorescent proteins (Cherry, Orange, or Cerulean), harvested at E18, and co-stained with CGRP to identify NE cell clusters.

[2] Number and color of cells in cluster determined by high-resolution confocal z-stacks through cluster. All miniclusters (clusters 1-4) and NEBs (clusters 5-12) examined were composed of cells of all three colors; similar results obtained for >100 additional clusters analyzed by conventional fluorescence microscopy.

**Table S2.** Clonal Analysis of NE Cell Progenitors, Related to Figure 3

Table S2A. Very sparse labeling and full analysis of NE clusters

| NE cluster[1] | No. of cells[2] | Ch cells[2] | Or cells[2] | Ce cells[2] |
|---|---|---|---|---|
| 1 | 8 | 0 | 1 | 0 |
| 2 | 10 | 0 | 1 | 0 |
| 3 | 12 | 0 | 0 | 0 |
| 4 | 20 | 0 | 0 | 0 |
| 5 | 20 | 0 | 0 | 0 |
| 6 | 21 | 0 | 0 | 0 |
| 7 | 25 | 0 | 0 | 0 |

[1] NE progenitors labeled by injection of *Ascl1*$^{CreER/+}$; *Rosa26*$^{Rbw/+}$ mice with 4 mg tamoxifen (E11.5). Lungs harvested at E17.5, and stained for CGRP (NE cells). Few NE progenitors express Ascl1 at induction, and only two labeled airway epithelial cells (yellow) were identified in entire lung. Cluster 1 is a mini-cluster and 2-7 are NEBs. Cluster 2 is shown in Figure 3B.
[2] Number and color (Ch, Cherry; Or, Orange; Ce, Cerulean) of NE cells in cluster.

Table S2B. Sparse labeling and partial analysis of NE clusters

| NE cluster[1] | No. of cells[2] | Ch cells[2] | Or cells[2] | Ce cells[2] |
|---|---|---|---|---|
| 1 | 1 | 0 | 0 | 0 |
| 2 | 2 | 0 | 0 | 0 |
| 3 | 2 | 0 | 0 | 0 |
| 4 | 2 | 0 | 0 | 0 |
| 5 | 2 | 1 | 0 | 0 |
| 6 | 2 | 0 | 0 | 0 |
| 7 | 2 | 0 | 0 | 0 |
| 8 | 3 | 0 | 0 | 0 |
| 9 | 3 | 0 | 0 | 0 |
| 10 | 3 | 0 | 0 | 0 |
| 11 | 3 | 0 | 0 | 0 |
| 12 | 4 | 0 | 0 | 0 |
| 13 | 4 | 0 | 0 | 0 |
| 14 | 4 | 0 | 0 | 0 |
| 15 | 4 | 0 | 0 | 0 |
| 16 | 4 | 1 | 1 | 0 |
| 17 | 5 | 0 | 0 | 0 |
| 18 | 5 | 0 | 0 | 0 |
| 19 | 5 | 0 | 0 | 0 |
| 20 | 5 | 0 | 0 | 0 |
| 21 | 5 | 0 | 0 | 0 |
| 22 | 5 | 0 | 1 | 1 |
| 23 | 5 | 0 | 0 | 0 |
| 24 | 5 | 0 | 0 | 0 |
| 25 | 5 | 0 | 0 | 0 |
| 26 | 5 | 0 | 0 | 0 |
| 27 | 6 | 0 | 0 | 0 |
| 28 | 6 | 0 | 0 | 0 |
| 29 | 6 | 0 | 0 | 0 |
| 30 | 6 | 0 | 0 | 0 |
| 31 | 6 | 0 | 0 | 1 |
| 32 | 6 | 0 | 0 | 0 |
| 33 | 6 | 0 | 0 | 1 |
| 34 | 6 | 0 | 1 | 0 |
| 35 | 6 | 0 | 1 | 0 |
| 36 | 7 | 0 | 0 | 0 |
| 37 | 7 | 1 | 0 | 0 |
| 38 | 7 | 0 | 0 | 0 |
| 39 | 7 | 0 | 0 | 0 |
| 40 | 7 | 0 | 0 | 0 |
| 41 | 7 | 0 | 1 | 0 |
| 42 | 8 | 0 | 0 | 0 |
| 43 | 8 | 0 | 0 | 0 |
| 44 | 8 | 0 | 1 | 1 |
| 45 | 8 | 0 | 0 | 1 |
| 46 | 8 | 0 | 0 | 0 |
| 47 | 16 | 0 | 0 | 0 |
| Total | 247 | 3 | 6 | 5 |

[1] NE progenitors were labeled as in Table S2A except 3 mg tamoxifen was injected at E12.5, when more NE progenitors express Ascl1. All NE clusters along left primary bronchus were scored.
[2] Number and color of NE cells in cluster as in Table S2A except only a single focal plane was examined per cluster. Miniclusters and NEBs were not distinguished, although clusters 42-47 are most likely NEBs. No clusters contained 2 cells of same color. Calculated labeling efficiency: Cherry (3 of 247 scored cells, 1.2%), Orange (2.4%), and Cerulean (2%), combined (5.6%).

Table S2C. Less sparse labeling and partial analysis of NE clusters

| NE cluster[1] | No. of cells[2] | Ch cells[2] | Or cells[2] | Ce cells[2] |
|---|---|---|---|---|
| 1 | 1 | 0 | 0 | 0 |
| 2 | 1 | 0 | 0 | 0 |
| 3 | 1 | 0 | 1 | 0 |
| 4 | 1 | 0 | 1 | 0 |
| 5 | 1 | 0 | 0 | 0 |
| 6 | 1 | 0 | 0 | 0 |
| 7 | 2 | 0 | 0 | 0 |
| 8 | 2 | 0 | 0 | 0 |
| 9 | 2 | 0 | 0 | 0 |
| 10 | 2 | 0 | 0 | 0 |
| 11 | 2 | 0 | 0 | 0 |
| 12 | 2 | 0 | 0 | 0 |
| 13 | 2 | 0 | 0 | 0 |
| 14 | 2 | 0 | 0 | 0 |
| 15 | 2 | 0 | 0 | 0 |
| 16 | 2 | 0 | 0 | 0 |
| 17 | 2 | 0 | 0 | 0 |
| 18 | 2 | 0 | 0 | 0 |
| 19 | 2 | 1 | 0 | 0 |
| 20 | 2 | 1 | 0 | 0 |
| 21 | 2 | 0 | 1 | 0 |
| 22 | 2 | 0 | 1 | 0 |
| 23 | 2 | 0 | 1 | 0 |
| 24 | 2 | 0 | 1 | 0 |
| 25 | 2 | 0 | 1 | 0 |
| 26 | 2 | 0 | 1 | 0 |
| 27 | 3 | 0 | 0 | 1 |
| 28 | 3 | 2 | 0 | 0 |
| 29 | 3 | 0 | 1 | 2 |
| 30 | 3 | 0 | 0 | 0 |
| 31 | 3 | 0 | 0 | 1 |
| 32 | 3 | 0 | 0 | 0 |
| 33 | 3 | 0 | 0 | 0 |
| 34 | 3 | 0 | 0 | 0 |
| 35 | 3 | 0 | 1 | 0 |
| 36 | 3 | 1 | 0 | 0 |
| 37 | 3 | 0 | 0 | 0 |
| 38 | 3 | 0 | 0 | 0 |
| 39 | 3 | 0 | 0 | 0 |
| 40 | 3 | 0 | 0 | 0 |
| 41 | 4 | 0 | 2 | 0 |
| 42 | 4 | 0 | 0 | 0 |
| 43 | 4 | 0 | 1 | 1 |
| 44 | 4 | 0 | 1 | 0 |
| 45 | 4 | 0 | 1 | 0 |
| 46 | 4 | 0 | 0 | 0 |
| 47 | 4 | 0 | 0 | 1 |
| 48 | 4 | 0 | 0 | 0 |
| 49 | 4 | 2 | 1 | 0 |
| 50 | 4 | 0 | 1 | 0 |
| 51 | 4 | 0 | 1 | 0 |
| 52 | 4 | 0 | 0 | 0 |
| 53 | 4 | 0 | 1 | 0 |
| 54 | 5 | 0 | 1 | 0 |
| 55 | 7 | 0 | 1 | 0 |
| Total | 152 | 7 | 21 | 6 |

[1] NE progenitors labeled as in Table S2B except with 4 mg tamoxifen.
[2] Number and color of NE cells determined as in Table S2B. Labeling efficiency: Cherry (4.6%), Orange (13.8%), Cerulean (3.9%), combined (22.3%); the expected number of clusters with more than one cell of same color (magenta) due to independent recombination events is 4, the same as the number observed.

**Table S3.** Schematics of NE Cell Intermediates Scored in Developing NEBs[1], Related to Figure 5

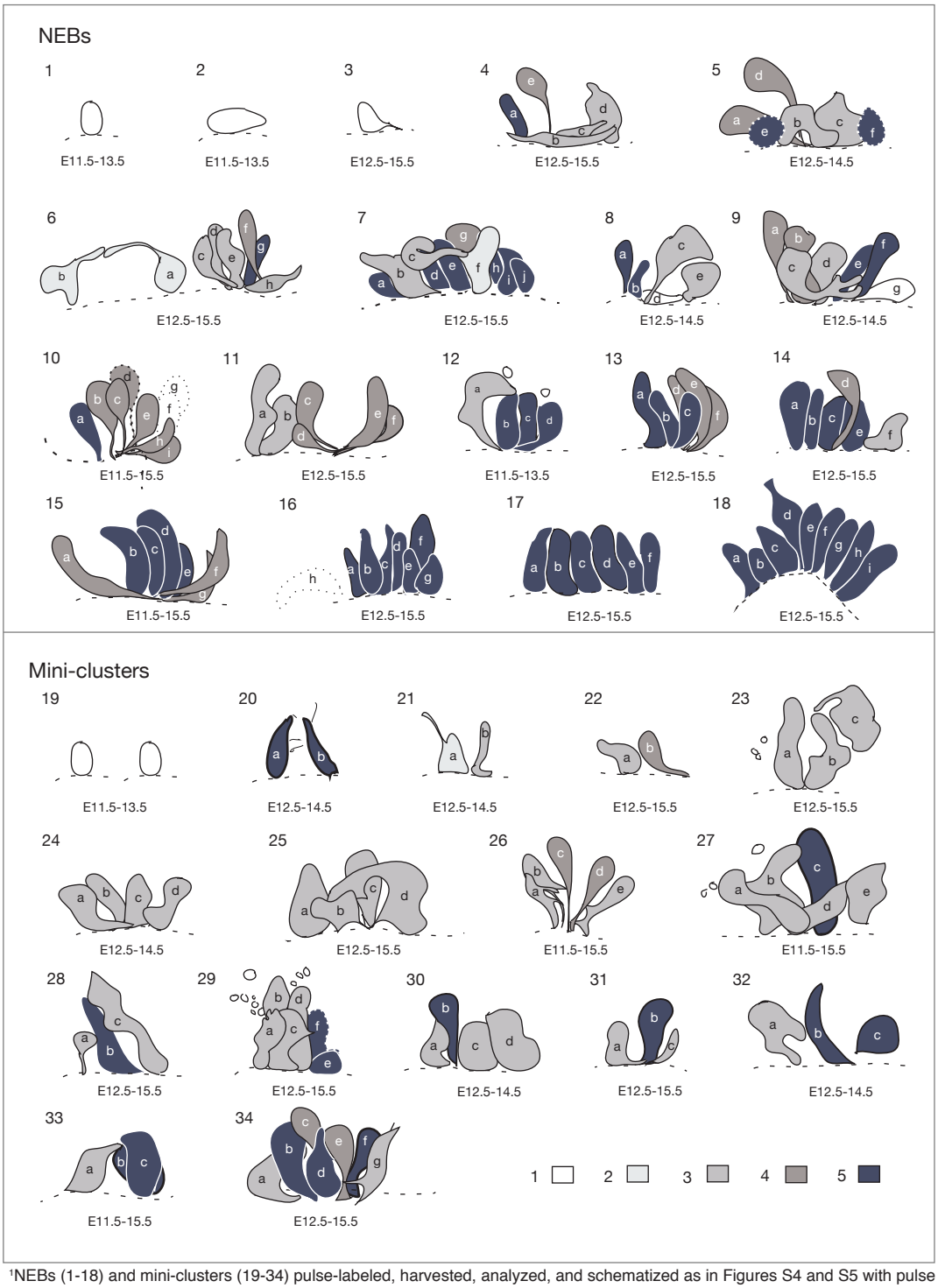


[1]NEBs (1-18) and mini-clusters (19-34) pulse-labeled, harvested, analyzed, and schematized as in Figures S4 and S5 with pulse (tamoxifen induction day) and harvest day indicated below each schematic.

**Supplemental References**

Danielian, P.S., Muccino, D., Rowitch, D.H., Michael, S.K., and McMahon, A.P. (1998). Modification of gene activity in mouse embryos in utero by a tamoxifen-inducible form of Cre recombinase. Curr. Biol. *8*, 1323–1326.

Harfe, B.D., Scherz, P.J., Nissim, S., Tian, H., McMahon, A.P., and Tabin, C.J. (2004). Evidence for an expansion-based temporal Shh gradient in specifying vertebrate digit identities. Cell *118*, 517–528.

Kim, E.J., Ables, J.L., Dickel, L.K., Eisch, A.J., and Johnson, J.E. (2011). Ascl1 (Mash1) defines cells with long-term neurogenic potential in subgranular and subventricular zones in adult mouse brain. PLoS ONE *6*, e18472.

Madisen, L., Zwingman, T.A., Sunkin, S.M., Oh, S.W., Zariwala, H.A., Gu, H., Ng, L.L., Palmiter, R.D., Hawrylycz, M.J., Jones, A.R., et al. (2010). A robust and high-throughput Cre reporting and characterization system for the whole mouse brain. Nat Neurosci *13*, 133–140.

Metzger, R.J., Klein, O.D., Martin, G.R., and Krasnow, M.A. (2008). The branching programme of mouse lung development. Nature *453*, 745–750.

Muzumdar, M.D., Tasic, B., Miyamichi, K., Li, L., and Luo, L. (2007). A global double-fluorescent Cre reporter mouse. Genesis *45*, 593–605.

Park, E.J., Sun, X., Nichol, P., Saijoh, Y., Martin, J.F., and Moon, A.M. (2007). System for tamoxifen-inducible expression of cre-recombinase from the Foxa2 locus in mice. Dev. Dyn. *237*, 447–453.

Rinkevich, Y., Lindau, P., Ueno, H., Longaker, M.T., and Weissman, I.L. (2011). Germ-layer and lineage-restricted stem/progenitors regenerate the mouse digit tip. Nature *476*, 409–413.

Rukstalis, J.M., and Habener, J.F. (2007). Snail2, a mediator of epithelial-mesenchymal transitions, expressed in progenitor cells of the developing endocrine pancreas. Gene Expression Patterns *7*, 471–479.